THE UNIVERSITY OF READING

A New Method for Solving the 2-D Advection Equation

by

Alistair Laird

Numerical Analysis Report 3/2000

The University of Reading
P.O. Box 220
Reading RG6 6AX
Berkshire, UK

DEPARTMENT OF MATHEMATICS

Abstract

This project investigates the use of upwind fluctuation distribution schemes to solve the 2D scalar advection equation, mainly concentrating on triangular grids, although basic quadrilateral grids are also analysed for the purpose of comparison.

Grid adaption is touched upon with the idea of the grid cells' edges having a prefered orientation with respect to the flow direction. Runge-Kutta (RK) time-stepping is used on time-dependent problems causing schemes to approach their steady state orders, and Flux-Corrected Transport (FCT) is used to produce monotone high order schemes.

Finally, a new scheme, third order accurate in space, is investigated. It is found to have a preferred grid, and reaches third order accuracy for time-dependent problems when equipped with third order RK time-stepping. For steady state problems, an FCT-type algorithm is proposed which switches between the new scheme and a traditional FCT algorithm to ensure a maximal order monotone scheme.

Acknowledgements

I would like to thank the EPSRC for their generous financial support this year, preventing many of the usual worries of university life.

I extend my gratitude to Prof. Mike Baines and Dr. Pete Sweby, ably assisted by Mrs Sue Davies, for organising a fascinating years study and always being available for consulatation, and Dr Matthew Hubbard for giving the inspiration for this project. Also my course friends: we all got on extremely well and helped each other out throughout the year. I wish them all every success in their future lives.

Finally, I would like to thank all the other friends I have met during my year's study at Reading, for some great times, and also my family for their continual support.

Contents

1 Introduction

A certain class of cell vertex finite volume schemes was introduced by Roe [1] in the early 1980s, with the aim of solving the 2D scalar advection equation numerically. Consequently developed further by that author and a number of others - most notably at the Von Karman Institute for Fluid Dynamics in Belgium - the schemes are now applicable in 3 dimensions, using systems of equations over many types of cells, working to a high degree of accuracy and stability, especially for steady state flows.

Known as multidimensional fluctuation distribution schemes (or some variation of) - whether they are classified as Finite Difference (FD), Finite Volume (FV), or Finite Element (FE) methods often depends on ones own perception. For instance, the use of a piecewise linear solution is the idea underlying FE methods, whilst the terms such as control volumes and monotonicity originate from the FV schemes. How to best describe these schemes is academic, but the fact that a variety of FD, FV and FE schemes may be written in the form of a fluctuation distribution scheme offers a medium for comparing and possibly improving various features of such methods.

For 1D advection, upwind schemes have been developed and proven to be both reliable and accurate methods, with guaranteed positivity. These Godonov type methods, first introduced in [3], involve the solution being cell-based and solving a Riemann problem at the cell boundaries. Second order accuracy can be assured when coupled with monotonicity preserving features such as flux limiting to produce so-called high resolution TVD schemes [4].

Extending into two-dimensions was originally 'achieved' by assuming 1D Riemann problems perpendicular to cell interfaces, and again using Godunov type methods. However, this led to a considerable loss of accuracy.

The problem of genuine 2D upwinding has been resolved by assuming a continuous piecewise approximate solution and defining a fluctuation for each cell which can be thought of as the distance of that cell from equilibrium. The method consequently distributes this fluctuation (sends a signal in the language of [1]) to the cell nodes in order to move closer to equilibrium.

These upwind fluctuation distribution schemes, solved on a compact stencil, generally produce second order accurate monotone solutions in the steady state, but only first order for time-dependent flows. One solution of the latter problem is by reconstructing the FE weighting functions corresponding to the space discretizations to form a consistent mass matrix [5]. In this project one idea is to combine a second order scheme (e.g. Lax Wendroff) with a lower order scheme (e.g. PSI) to get the benefits of them both. This is done in the form of an FCT algorithm [6] [7] [8], or the more general fluctuation redistribution method of [9], both being 2D forms of the TVD flux limiting schemes mentioned earlier. Another idea is to replace the simple first order Euler time-stepping of a scheme such as PSI with a higher order TVD

Runge-Kutta time-step as used in [21], in the hope that the time-step will not dominate the truncation error, hence leaving the order of accuracy spatially dependent, i.e. the order at steady state. Both of these two ideas are met in Chapter 5.

The schemes can be applied on triangles or quadrilaterals, but the majority of the work carried out in this project will be concentrated on triangular grids with their greater degree of flexibility. This is introduced in Chapter 2 and represents the most thoroughly researched area of fluctuation distribution schemes. However it must be pointed out that structured triangular grids are generally used, although all the methods, and most of the results still apply for any arbitrary triangulation. The structure of these grids ensures an underlying square grid when the diagonals are removed, and provides an opportunity to compare schemes, devised in similar ways, on both types of grids, (Chapter 3).

Such comparisons pave the way for a greater understanding of triangular grids and bring forward the idea of a basic form of grid adaption. Making the following definition:

Let ψ be the smallest angle between the advection velocity $\vec{\lambda}$, and the diagonal part of the triangular cell (see Figure 1).

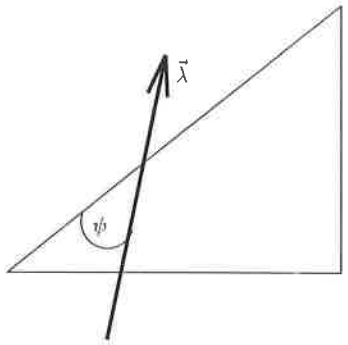

Figure 1: The angle ψ

If	$\lvert\frac{\pi}{4}\rvert \leq \psi$	then the flow is in the SAME direction as the diagonals,
	$\lvert\frac{\pi}{4}\rvert \geq \psi$	then the flow is in the OPPOSITE direction to the diagonals.

It is well known that the direction of the diagonals can affect the performance of a scheme, hence the idea of changing these diagonals to create a grid which enhances a scheme's performance is looked at in Chapter 4.

In an attempt to gain further accuracy, in this project a new third order fluctuation distribution scheme, proposed by Hubbard (private communication) is investigated in Chapter 6. Devised on an extended stencil, the basic scheme suffers from instabilities as well as a low

order of accuracy for time-dependent problems. The idea in this work is to investigate and attempt to improve the scheme using the framework set out in the preceding chapters.

2 Fluctuation Distribution Schemes on 2D Triangular Grids

In [1], in an attempt to find a set of 'rules' to generate good numerical models of evolutionary problems found in physics, Roe introduces two basic concepts:

- *fluctuation* is something detected in the data, indicating that it has not yet reached equilibrium.
- *signal* is an action performed on the data so as to bring it closer to equilibrium.

These two, very basic ideas are the basis of the fluctuation distribution methods.

Consider solving the homogeneous advection equation in 2D,

$$u_t + f_x + g_y = 0 \qquad \text{or}$$

$$u_t + \vec{\lambda}.\vec{\nabla}u = 0 \tag{1}$$

on a triangulated domain, using a numerical method.
Here $\vec{\lambda} = \left(\frac{\partial f}{\partial u}, \frac{\partial g}{\partial u}\right)^T$, the advection velocity may be:

1. Constant - linear advection.
2. Function of x, y - non-uniform linear advection.
3. Function of u - non-linear conservation law.

Following on from FE methodology, a continuous piecewise linear approximation to the exact solution is constructed in the plane. The approximate nodal solutions are stored at the triangles' vertices. Supposing these nodes have coordinates (x_i, y_i) the solutions have representations of the form

$$u(x, y, t) = \sum_i u_i(t) w_i(x, y)$$

where $w_i(x_i, y_i) = 1$
$w_i(x_i, y_i) = 0$ for $i \neq j$
w_i is continuous and piecewise linear over the domain.Hence w_i is a typical piecewise linear basis function as met in FEs.

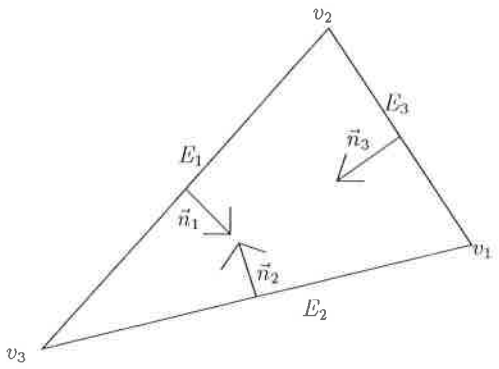

Figure 2: Labelling of a typical triangle

Now, consider an arbitrary triangle in isolation with vertices v_1, v_2, v_3, and corresponding edges E_1, E_2, E_3, and normals to these edges $\vec{n}_1, \vec{n}_2, \vec{n}_3$, (see Figure 2). For any such triangular cell, its fluctuation is defined as

$$\begin{aligned} \phi_T &= \iint_{\triangle} u_t \, \mathrm{d}x \, \mathrm{d}y \\ &= -\iint_{\triangle} \vec{\lambda}.\vec{\nabla} u \, \mathrm{d}x \, \mathrm{d}y \\ &= \oint_{\partial\triangle} u\vec{\lambda}.d\vec{n} \end{aligned} \tag{2}$$

where $\partial\triangle$ is the boundary of the triangle,

$\vec{n}$ is the scaled inward normal to the boundary.

Since u has been assumed to vary linearly across $\triangle$, then,

$$\begin{aligned} \phi_T &= -S_T \vec{\lambda}.\vec{\nabla} u \\ &= -\sum_{i=1}^{3} u_i k_i \end{aligned} \tag{3}$$

where S_T is the area of the triangle,

$k_i = \frac{1}{2}\vec{\lambda}.\vec{n}_i$.

Throughout the development of these schemes, special care is paid to maintaining conservation of the solution, i.e.

$$\iint_{domain} u_t \, \mathrm{d}x \, \mathrm{d}y = \sum_{all\triangle's} \iint_{\triangle} u_t \, \mathrm{d}x \, \mathrm{d}y.$$

In determining the fluctuation (3), the piecewise linear solution is sufficient in the linear advection case, with a cell-wise local velocity being used in the non-constant case.

For the non-linear case,

$$u_t + f(u)_x + g(u)_y = 0,$$

an equivalent linear problem is defined in each cell. One consistent, conservation maintaining linearised advection velocity, $\widehat{\vec{\lambda}}$, from [10] and used in this project, is obtained as follows. For the arbitrary cell in Figure 3,

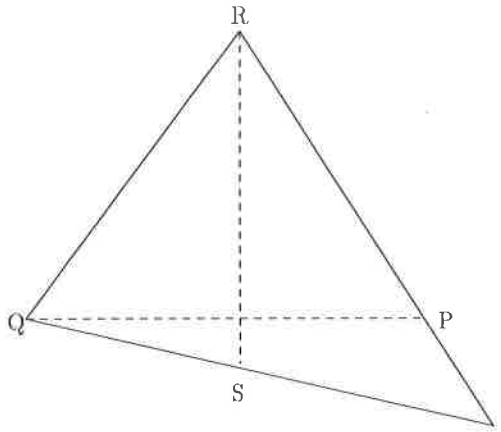

Figure 3: Labelling for the non-linear advection linearisation.

$$\widehat{\vec{\lambda}} = \begin{pmatrix} \tilde{a} \\ \tilde{b} \end{pmatrix} \qquad \text{where} \qquad \tilde{a} = \frac{f_P - f_Q}{u_P - u_Q} \qquad \tilde{b} = \frac{g_R - g_S}{u_R - u_S} \tag{4}$$

where f_P, g_S, u_P, u_S are obtained by linear interpolation along the edges.

The computation of the k_i's in (3) has the added advantage of telling us the direction of flow through a cell, with:

- $k_i > 0 \Rightarrow E_i$ is an inflow edge.
- $k_i < 0 \Rightarrow E_i$ is an outflow edge.
- $k_i = 0 \Rightarrow$ flow is parrallel to E_i.

This is used later in devising schemes, and is especially useful in coding schemes with non-constant flow.

With the fluctuation known, a signal must be sent to the triangles nodes in an attempt to reduce the fluctuation. This is done by sending the cell's fluctuation to the nodes of the cell using *distribution coefficients*,

$\alpha_{T,i}$ - the proportion of ϕ_T sent to node i.

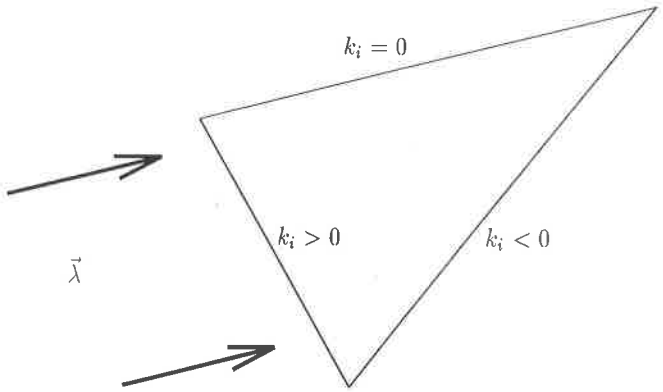

Figure 4: Flow through a typical triangle

For schemes so far proposed, the fluctuation is distributed to nodes of the cell from which it came. Hence, we have a scheme which is computationally compact, and so cells may be considered in isolation with the resulting possibilities of parallel computing and all the efficiency advantages that brings. Also, in order to maintain conservation at distribution, no fluctuation should be lost or gained, i.e.

$$\sum_{i=1}^{3} \alpha_{T,i} = 1 \quad \forall\, T$$

Bearing in mind that a node may receive signals from all its adjacent $\triangle$s, and using simple Euler time-stepping, we get the general fluctuation distribution scheme,

$$u_i^{n+1} = u_i^n + \frac{\triangle t}{S_i} \sum_T \alpha_{T,i} \phi_T$$

where S_i is the area of the median dual cell surrounding node i.

Note: i is a global numbering system. Since ϕ_T is only distributed to the nodes of T, $\alpha_{T,i} = 0$ if i is not on T.

So it is the choice of α's which defines an individual scheme. Such coefficients are chosen with the usual considerations of stability, accuracy, simplicity etc. in mind.

We have 3 design criteria which are desirable for any fluctuation distribution scheme to possess:

1. *Continuity* - this requires that the distribution coefficients $\alpha_{T,i}$ be continuous for changes in both the advection velocity $\vec{\lambda}$, and the solution itself.

2. *Positivity*(P) - if a scheme is written in the form

$$u_i^{n+1} = \sum_l c_l u_l^n \qquad , \qquad \text{where } c_l \text{ is independent of the data,}$$

then the scheme is positive if $c_l \geq 0$ for all l. This guarantees that a maximum principle is obeyed, which prohibits the occurrence of new extrema at the next time level, provided a CFL-like condition is obeyed.

There is a fair amount of ambiguity in describing schemes which do not generate new extrema. In this project, a scheme which possesses this property will be refered to as monotone.

3. *Linear Preservation*(LP) - this requires that when the exact steady state solution is a linear function of x and y, for any triangulation the scheme preserves this exact solution. In [14] it is shown that a necessary and sufficient condition for an LP scheme is that the $\alpha_{T,i}$'s are bounded as $\phi_T \longrightarrow 0$. LP schemes tend to be very accurate, in fact they suffer from no cross-wind diffusion and are second order accurate at the steady state [14]. However, if not equipped with positivity, they may suffer from spurious oscillations.

2.1 Upwind schemes

Upwind fluctuation distribution schemes are those which only send contribution to the downstream nodes. Using the introduced nomenclature, this can be written as,

$$\alpha_{T,i} = 0 \qquad \text{if} \qquad k_i < 0$$

This leads to 2 possibilities:

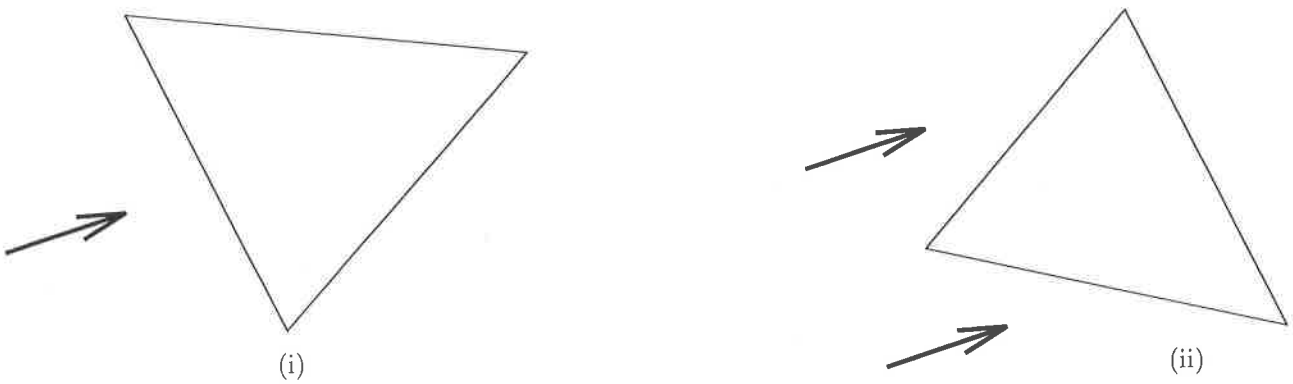

Figure 5: (i) 1 inflow edge, (ii) 2 inflow edges

(i) All the fluctuation is distributed to the single downstream node.

(ii) Fluctuation is shared between the 2 downstream nodes.

Now, it is desired to find schemes which satisfy as many of the design criteria as possible, although it should be noted that it has been proven in [11] that no linear scheme can be both positive and linear preserving.

2.1.1 Linear Schemes

These schemes are linear in the sense that the distribution coefficients ($\alpha_i's$) are independent of the data ($u_i's$). For all such schemes, as stated before, when we have one inflow side then all the fluctuation is distributed to the downstream node. This strategy is both LP and P satisfying. So what distinguishes the schemes is the splitting of the fluctuation where we have 2 downstream nodes.

The LDA Scheme

The Low-Diffusion Scheme A (LDA) [12] is a straightforward, linear, LP (hence non-positive) scheme derived from splitting the triangle into 2 parts. Assuming the fluctuation to be uniform across the triangle, it is split into 2 by the velocity vector passing through the upstream node.

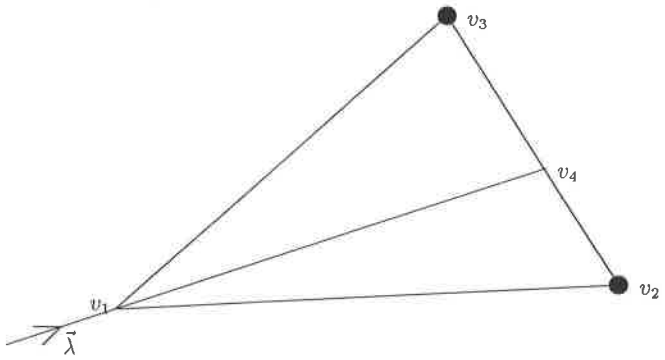

Figure 6: $\vec{\lambda}$ passing through v_1, splitting up the triangle.

The respective fluctuations in each triangle is distributed to the downstream nodes ($\bullet$) in that triangle. So using the triangle in Figure 6,

$$\begin{aligned} \alpha_1 &= 0, \\ \alpha_2 &= \frac{\text{Area}\triangle 143}{\text{Area}\triangle 123}, \\ \alpha_3 &= \frac{\text{Area}\triangle 124}{\text{Area}\triangle 123}, \end{aligned}$$

which, after some working results in

$$\alpha_1 = 0,$$

$$\alpha_2 = -\frac{k_2}{k_1},$$
$$\alpha_3 = -\frac{k_3}{k_1}.$$

Now, $\alpha_1 + \alpha_2 + \alpha_3 = 1$, so conservation is maintained and, due to the LP property, steady state results show very low cross diffusion, hence the scheme's name.

The N Scheme

The Narrow (N) scheme [12] is the optimum linear positive scheme for minimising cross-wind diffusion. It is obtained by adding parameters to create a general scheme and fixing these to ensure positivity. It is however far nicer explained geometrically, like the previous case. Firstly, let the advection velocity be expressed in terms of 2 vectors: $\vec{\lambda_2}$ parallel to E_2 and $\vec{\lambda_3}$ parallel to E_3, such that,

$$\vec{\lambda} = \vec{\lambda_2} + \vec{\lambda_3}$$

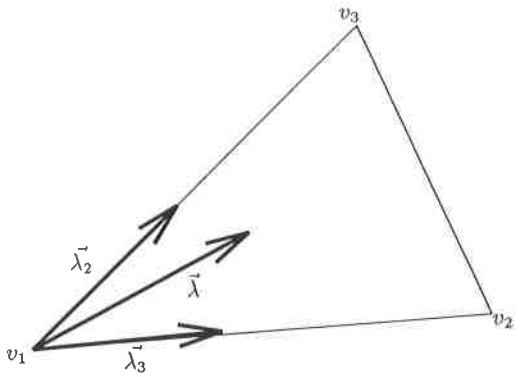

Figure 7: $\vec{\lambda}$ and its 2 component parts.

Now, thinking of $\vec{\lambda_2}$ as sending some fluctuation to v_3, and $\vec{\lambda_3}$ sending fluctuation to v_2.

Using the result,

$$k_1 + k_2 + k_3 = 0,$$

and equation (3), the fluctuation may be written as

$$\begin{aligned} \phi_T &= -k_2(u_2 - u_1) - k_3(u_3 - u_1) \\ &= -\frac{1}{2}(\vec{\lambda}.\vec{n_2})(u_2 - u_1) - \frac{1}{2}(\vec{\lambda}.\vec{n_3})(u_3 - u_1) \end{aligned} \tag{5}$$

So, thinking of v_3 receiving fluctuation via $\vec{\lambda_2}$, $\phi_{T,3}$ say $\Rightarrow$

$$\begin{aligned}\phi_{T,3} &= -\frac{1}{2}(\vec{\lambda_2}.\vec{n_2})(u_2-u_1) - \frac{1}{2}(\vec{\lambda_2}.\vec{n_3})(u_3-u_1) \\ &= -\frac{1}{2}(\vec{\lambda_2}.\vec{n_3})(u_3-u_1) \\ &= -\frac{1}{2}(\vec{\lambda}.\vec{n_3})(u_3-u_1) \\ &= -k_3(u_3-u_1). \end{aligned} \tag{6}$$

Similarly the fluctuation sent by $\vec{\lambda_3}$ gives

$$\phi_{T,2} = -k_2(u_2-u_1). \tag{7}$$

Also, for the purposes of comparison, the actual distribution coefficients as found in [13] can be written as

$$\alpha_{T,i} = \frac{\phi_i}{\phi_T} \tag{8}$$

where

$$\phi_i = -\frac{\max(0,k_i)}{\sum_{l=1}^{3}\max(0,k_l)}\sum_{j=1}^{3}\min(0,k_j)(u_i-u_j)$$

2.1.2 Non-linear Schemes

The PSI Scheme

A non-linear scheme combining positivity and linearity preservation and being theoretically[2] second order accurate at the steady state was derived by Struijs [14]. Called the Positive Streamwise Invariant (PSI) Scheme, its idea is to enforce invariance along streamlines (characteristics). To do this a characteristic must be pictured, going through the upstream node if there is only one such node, or through the downstream node otherwise.
The thinking now is to devise a scheme such that (see Figure 8)

$$u^{n+1}(\vec{r_{out}}) = u^n(\vec{r_{in}})$$

It was later shown in [15] that the PSI scheme could be written as a limited version of the N-scheme using the MinMod limiter. Looking at the case where we have two downstream

[2]It has been shown in [13] that the non-linearity causes a real order of accuracy of about 1.65

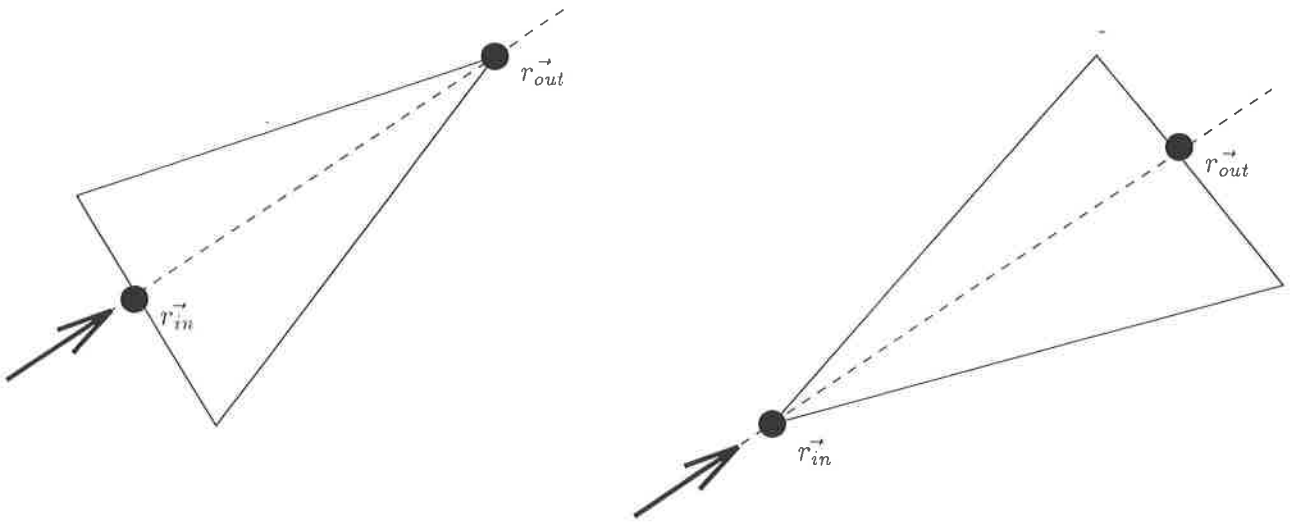

Figure 8: The position vectors as the characteristic enters and leaves the triangle.

nodes, let the contributions to these nodes be ϕ_1, ϕ_2 and ϕ_1^*, ϕ_2^* for the N scheme and the PSI scheme respectively. Then,

$$\begin{aligned} \phi_1^* &= \phi_1 - L(\phi_1, -\phi_2) \\ \phi_2^* &= \phi_2 - L(\phi_2, -\phi_1) \end{aligned} \tag{9}$$

where $L(x, y) : \Re^2 \longrightarrow \Re$ is the MinMod limiter.

$$L(x, y) = \frac{1}{2}(1 + \text{sign}(xy))\frac{1}{2}(\text{sign}(x) + \text{sign}(y)\min(|x|, |y|) \tag{10}$$

So, a linear positive scheme has been taken, and a limiter applied to add linearity preservation at the expense of the linearity of the scheme.

2.2 FE/FV Schemes

Although the following schemes are neither strictly upwind in the sense we used earlier nor developed with a fluctuation distribution context in mind, they often show an upwind bias and can be written in the form of a fluctuation distribution scheme, thus enabling us to compare with the newer upwind schemes.

The Lax-Wendroff Scheme

This is the unique single step, second order accurate, linear, LP fluctuation distribution

scheme [16]. One way of deriving it is by using a finite volume approach, making use of the Lax-Wendroff 'trick' of Taylor series expansions as follows:

1. Take the Taylor Series truncated to second order in time,

$$u^{n+1} \approx u^n + \triangle t u_t + \frac{1}{2}\triangle t^2 u_{tt}.$$

2. Substitute in the advection equation,

$$u^{n+1} - u^n \approx -\triangle t(au_x + bu_y) - \frac{1}{2}\triangle t^2(au_x + bu_y)_t. \tag{11}$$

3. Integrate over a 'control volume' - median dual cell, area S_p (equivalent to mass-lumping in FE).

4. Take a compact stencil of the form in Figure 9.

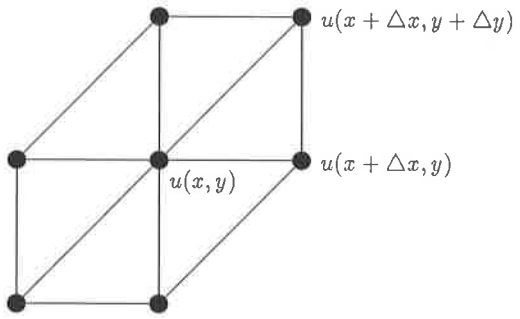

Figure 9: Compact stencil in consideration.

5. Write a linear combination of the above nodal values using unknown coefficients.

6. Expand these using Taylor Expansions.

7. Equate with (11) to find coefficients of nodes in the scheme to satisfy terms up to second order spatial accuracy.

This gives a scheme which can be written in fluctuation distribution form, with

$$\alpha_{T,i}^{LW} = \frac{1}{3} + \frac{1}{2}\triangle t \frac{k_i}{S_T}$$

where $k_i = \frac{1}{2}\vec{\lambda}.\vec{n_i}$

The Central FV Scheme

Taking a Taylor Series truncated to first order accuracy in time, i.e.

$$u^{n+1} \approx u^n + \triangle t u_t,$$

and using the same technique as with deriving the LW scheme we gain the Jameson central FV scheme [17] with

$$\alpha_{T,i} = \frac{1}{3}.$$

This can also be shown to be identical to the Galerkin FE method whereby the test functions used in the weak form are the element basis functions $w_i(x, y)$ introduced earlier, albeit with the additional use of mass lumping.

The complete lack of an upwind bias in this technique is reflected in the fact that it is unstable. Hence, leaving out the dissipative contribution in the derivation of the scheme has de-stabilized the scheme. Consequently, to recreate a stable scheme, a degree of dissipation has to be re-added to the scheme.

SUPG Schemes

Streamline-Upwind-Petrov-Galerkin (SUPG) FE methods [18] aim to stabilize the above method by re-introducing the dissipation in the test function $\tilde{w}_i$,

$$\tilde{w}_i = w_i + \tau_1 \vec{\lambda}.\vec{\nabla} w_i = w_i + \tau_1 \frac{k_i}{S_T}, \tag{12}$$

where w_i is the standard Galerkin test function,
τ_1 is a positive parameter.

Not surprisingly, depending on choice of τ_1, the LW scheme can be recovered via this technique (letting $\tau_1 = \frac{1}{2}\triangle t$). Again, using mass-lumping, this can be written as a fluctuation distribution scheme with distribution coefficients,

$$\alpha_{T,i} = \frac{1}{3} + \tau_1 \frac{k_i}{S_T}.$$

Thus, we have regained an element of upwinding from the second term which has the possible effect of stabilizing the scheme (depending on the choice of τ_1).

Hughes [18] has further improved the method by adding a non-linear discontinuity capturing term in the test function, $\breve{w}$,

$$\breve{w}_i = \tilde{w}_i + \tau_2 \vec{\lambda}\|.\vec{\nabla} w_i$$

where $\vec{\lambda}\|$ is a projection of the advection velocity,

τ_2 is a parameter.

Johnson's approach [19] was also to add this discontinuity capturing ter, but this time to the initial equation (1) itself, using an artificial viscosity (AV) term, $\hat{\kappa}^2$. So the modified equation to be solved is

$$u_t + \vec{\lambda}.\vec{\nabla}u = \vec{\nabla}.(\hat{\kappa}\vec{\nabla}u). \tag{13}$$

Taking

$$\hat{\kappa} = \frac{1}{2}\triangle x \frac{\vec{\lambda}.\vec{\nabla}u}{|\vec{\nabla}u| + \nabla x}$$

gives distribution coefficients

$$\alpha_{T,i} = \frac{1}{3} + \tau_1 \frac{k_i}{S_T} + \frac{1}{2}\triangle x \frac{|\vec{\nabla}u|(k_i)\|}{|\vec{\lambda}.\vec{\nabla}u|S_T} \tag{14}$$

where $(k_i)\| = \frac{1}{2}\vec{\lambda}\|.n_i$.

Returning to Hughes' method, he uses parameters

$$\tau_1 = \frac{1}{2}\frac{\triangle x}{|\vec{\lambda}|}, \qquad \tau_2 = \frac{1}{2}\frac{\triangle x}{|\vec{\lambda}|\|}.$$

One way of looking at the accuracy of a scheme is by assuming any errors in the scheme are equivalent to exactly solving a perturbed equation - the *Equivalent Equation.*

The *Equivalent Equation* is the differential equation that a numerical scheme actually solves, rather than one that it purports to solve [9].

This can be found using an approach like that of [9] whereby the concept of a distribution point is used.

This equivalent equation can be shown to be (13), hence Johnson's and Hughes' methods both produce the same monotone fluctuation distribution scheme with distribution coefficients (14), at least when solving the pure advection equation with constant velocity.

2.3 Numerical Results

The performacne of the schemes presented in this chapter is demonstrated on 4 test problems, chosen to investigate various essential aspects of such schemes. The solutions are computed over

a regular triangular grid with equi-distant nodal spacings of h=1/32 in both spatial directions. Unless otherwise stated the grid used will be of the type A below, although the other two are used to compare performance.

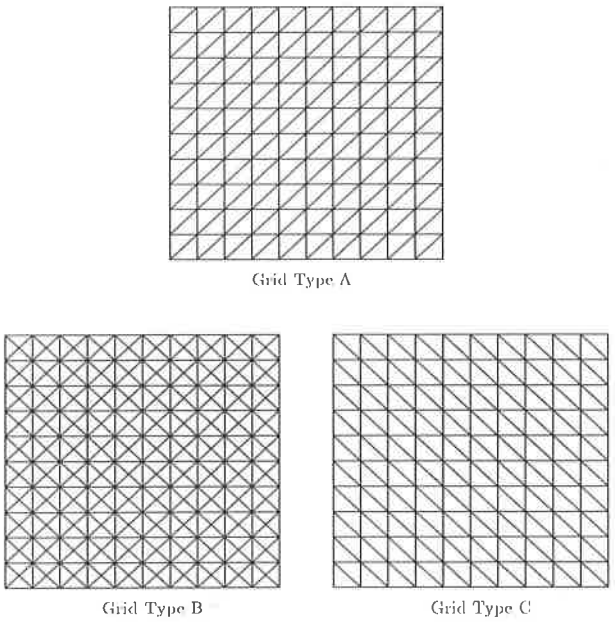

Figure 10: The grids used in this section

Firstly, a time-dependent periodical problem is investigated with the linear advection of a double sine curve. By allowing the problem to run for one time-period, the numerical accuracy of the schemes is investigated. In the next two problems, the schemes are left until the steady state is reached and their respective efficiencies in modelling discontinuities is analysed in the cases of firstly constant, then rotational advection. Finally, shock capturing properties are studied by means of a non-linear advection equation, coupled with boundary conditions which ensure the formation of a shock.

Constant Linear Advection

The first test case involves the advection of the double sine wave,

$$u = sin(2\pi x)sin(2\pi y) \tag{15}$$

with velocity $\vec{\lambda} = (1, 2)^T$ over the domain $(x, y) \in [0, 1]$x$[0, 1]$. Periodic boundary conditions are applied such that at t=1.0 the solution should have returned to its initial position.

Figure 11 shows the results of using five schemes with the CFL number of 0.72, comparing the solutions at t=1.0. The following observations can be made from figure 11 :

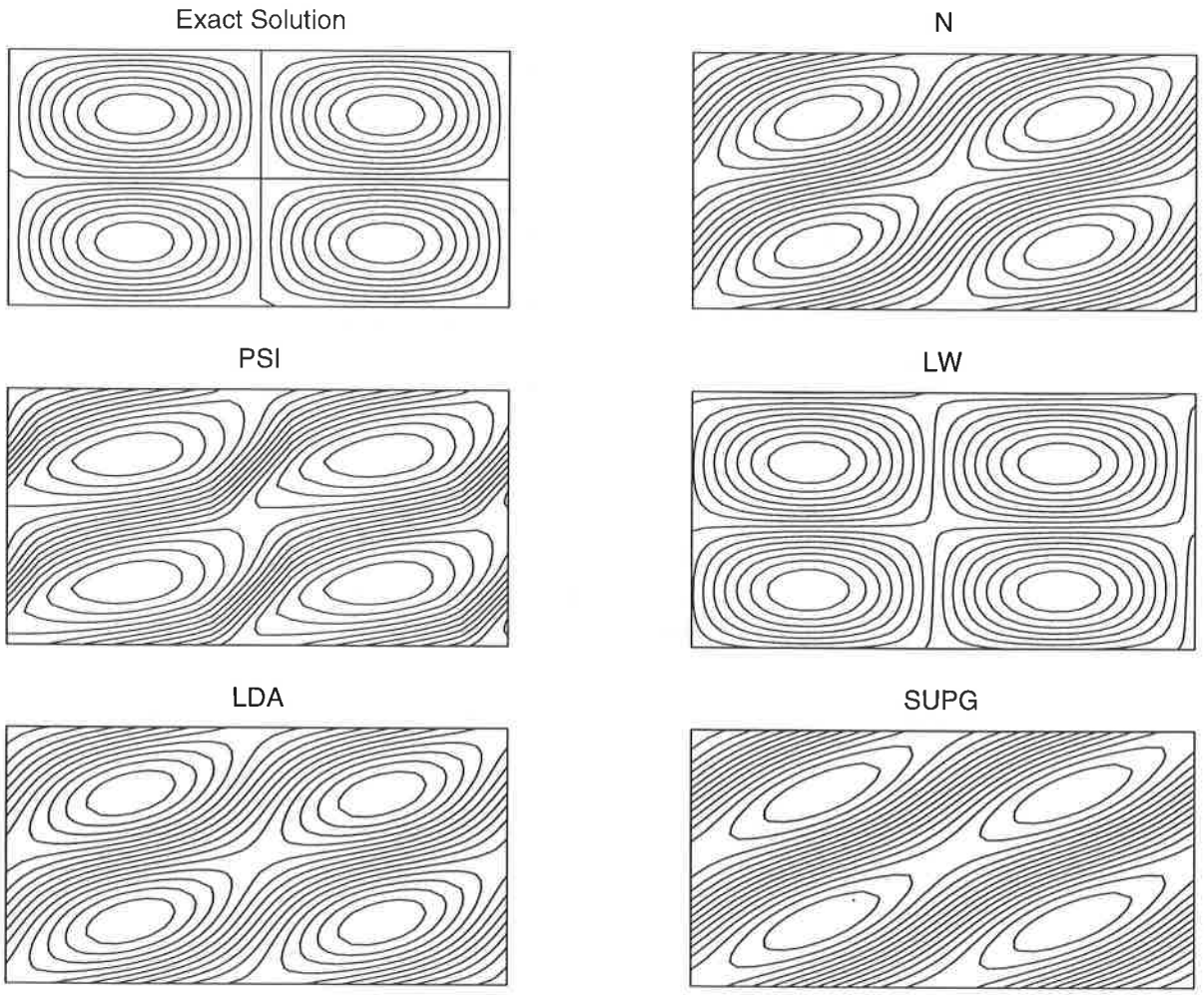

Figure 11: Advection of the double sine wave.

Scheme	CFL=0.716		CFL=0.358	
	L_1	L_{inf}	L_1	L_{inf}
LDA	0.83	0.85	0.70	0.73
LW	1.99	2.00	1.99	2.00
SUPG	0.69	0.73	0.98	0.00
PSI	0.76	0.81	0.64	0.71
N	0.78	0.82	0.66	0.72

Table 1: Numerical orders of accuracy in double sine-wave advection case.

1. LW seems to preserve the solution best, despite a slight phase lag.
2. The other 4 schemes appear to have the curves merging together.
3. Streamwise diffusion seems to be the problem in these 4 schemes, most notably in the SUPG scheme.
4. This diffusion is symmetric in both directions in all but the PSI scheme, which appears to have more diffusion in the upstream direction.

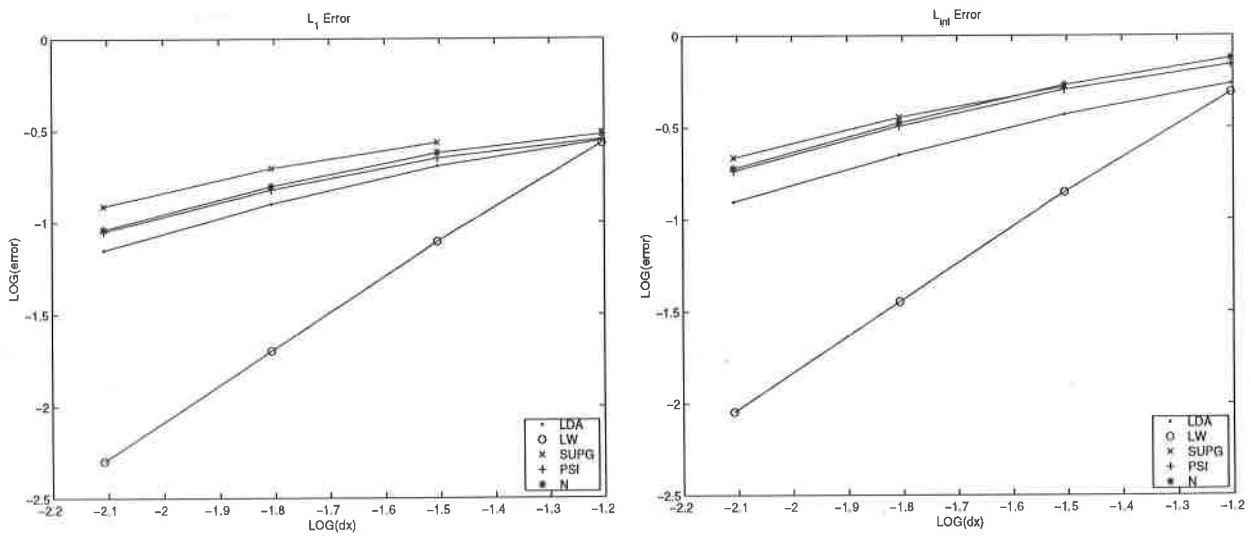

Figure 12: Graph of respective errors on Grid A

Figure 12 and Table 1 show the results of a numerical accuracy study by refining the grid, keeping the CFL number constant, and studying the norm of the error vector.

Not surprisingly from the visual results LW is the most accurate, reaching second order accuracy for this problem, as predicted by the theory. The other schemes achieve accuracy of

order between 0.5 and 1.0. One surprising result is that lowering the CFL number does not necessarily lower the accuracy as would be expected from the theory (especially in the linear case). This disagrees with numerical evidence in [5] which agrees with our initial thinking, but uses more complicated Crank-Nicolson time-stepping. So decreasing time-steps could only decrease error for some methods of discretising u_t.

Also worthy of note is the closeness of the orders of accuracy of the PSI and N schemes, implying that the MinMod limiter of the PSI scheme has minimal effect in this problem.

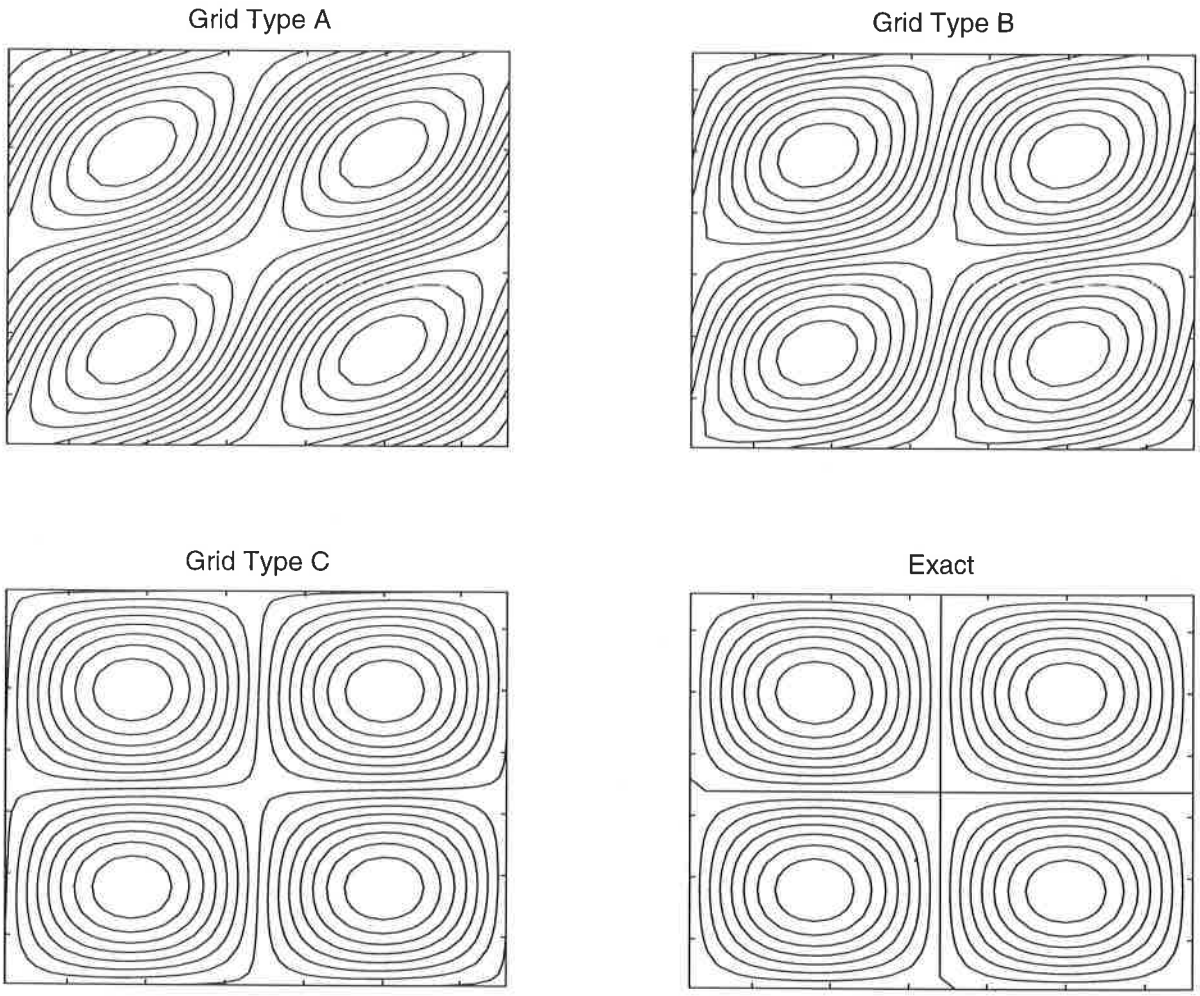

Figure 13: Advection of the double sine wave using the LDA scheme and different grids.

Figure 13 shows the results of using different grids on one scheme. From this the effect of the grid type is very noticeable. More specifically, when the triangles are pointing in the same direction as the velocity the scheme appears to suffer from streamwise diffusion (in the LDA case at least). This problem is solved by using triangles facing the other way, which is partially done in the Grid B case, and fully in Grid C.

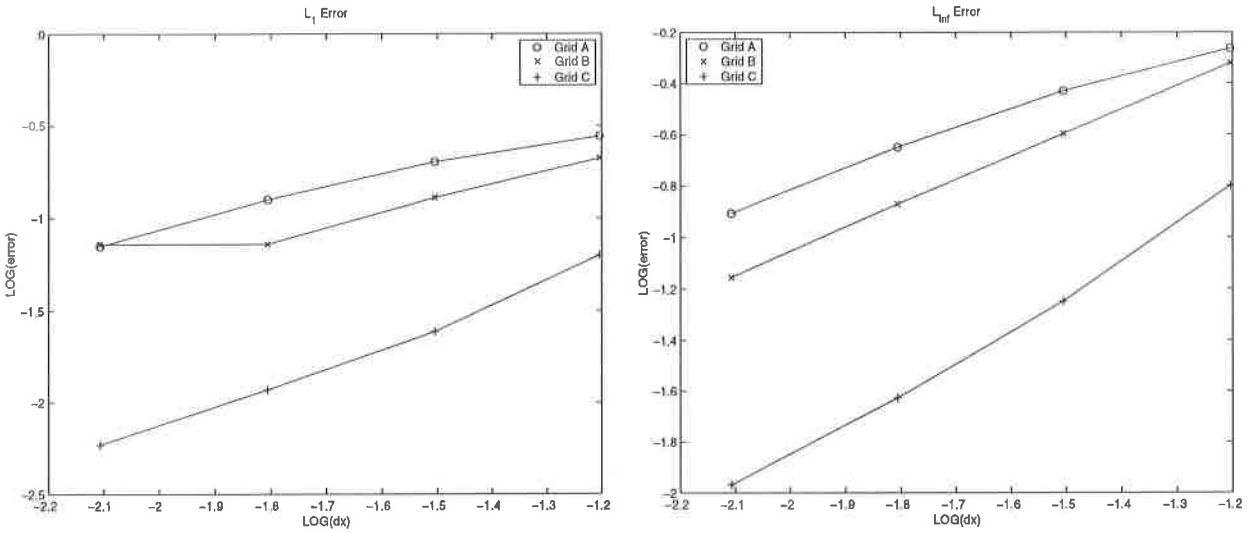

Figure 14: Errors for the advecting double sine-wave on Grid A.

Grid	L_1	L_{inf}
A	0.83	0.85
B	0.83	0.94
C	1.00	1.13

Table 2: Numerical orders of accuracy in double sine-wave advection case.

Figure 14 and Table 2 shows the results of a numerical accuracy study by refining the 3 grids using the LDA scheme. The numerical orders of accuracy match up with the visual evidence, i.e. for this particular problem the Type C grid is the most effective in modelling the solution.

Constant Linear Advection of a Discontinuous Solution

The second problem models a contact discontinuity with a discontinuous profile moving with speed $\vec{\lambda} = (sin\frac{\pi}{8}, cos\frac{\pi}{8})^T$, in the domain $(x, y) \in [0, 1]$x$[0, 1]$. The initial conditions are:

$$\begin{aligned} u(0, y) &= 1 \quad \text{for} \quad 0 \leq y \leq 1, \\ u(x, y) &= 0 \quad \text{for} \quad 0 < x \leq 1, \quad 0 \leq y \leq 1, \end{aligned} \tag{16}$$

with inflow boundary conditions:

$$\begin{aligned} u(0, y) &= 1 \quad \text{for} \quad 0 \leq y \leq 1, \\ u(x, 0) &= 0 \quad \text{for} \quad 0 < x \leq 1. \end{aligned}$$

Fig 15 shows the steady state solutions of six schemes described earlier with a CFL number of 0.32.

Circular Advection of a Discontinuous Solution

The third problem models a square waves convection around the origin with velocity $\vec{\lambda} = (y, -x)^T$, in the domain $(x, y) \in [-1, 1]$x$[0, 1]$. The initial conditions are:

$$\begin{aligned} u(x, 0) &= 1 \quad \text{for} \quad -0.65 \leq x \leq -0.35, \\ u(x, y) &= 0 \quad \text{elsewhere}, \end{aligned} \tag{17}$$

with inflow boundary conditions:

$$\begin{aligned} u(x, 0) &= 1 \quad \text{for} \quad -0.65 \leq x \leq -0.35, \\ u(x, 0) &= 0 \quad \text{for} \quad -1 < x \leq -0.65, \quad -0.35 < x \leq 0, \\ u(x, 1) &= 0 \quad \text{for} \quad 0 \leq x \leq 1, \\ u(0, y) &= 0 \quad \text{for} \quad 0 \leq y \leq 1. \end{aligned}$$

Figure 16 shows the steady state solutions of five schemes described earlier with a maximum CFL number of 0.45.

The following observations on discontinuity capturing can be made on the basis of the last two examples:

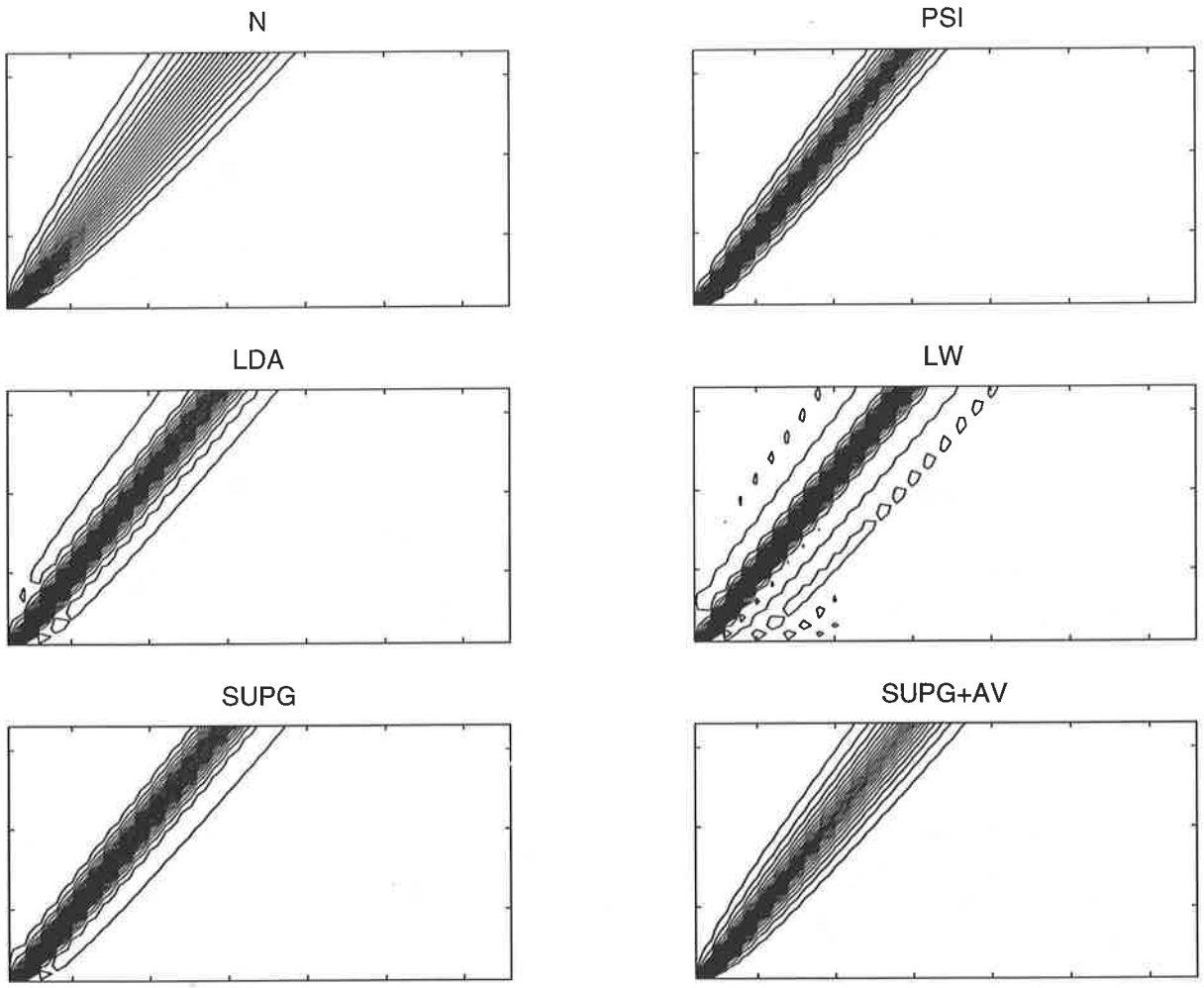

Figure 15: Linear advection of a discontinuity.

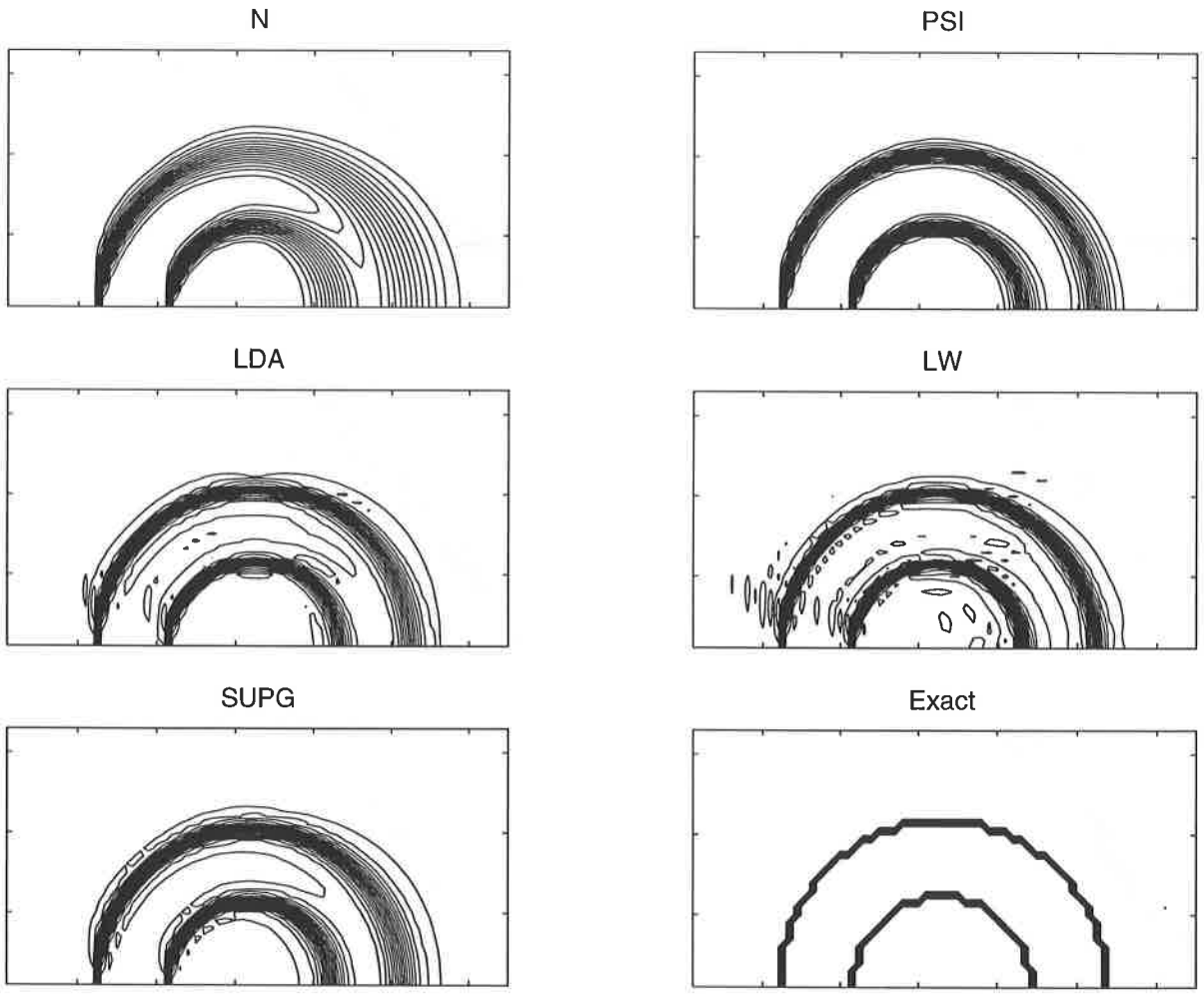

Figure 16: Circular advection of a discontinuity.

1. The N-scheme, being the only non-LP scheme on show, shows significantly more cross-wind diffusion than the other LP schemes.

2. The 3 non-positive scemes (LDA, LW, SUPG) all suffer from spurious oscillations around the discontinuity, with LW appearing to suffer the worse, followed by LDA then SUPG.

3. The artifical viscosity introduced in the SUPG+AV case has the affect of creating a monotone scheme (no over or undershoots) but increases cross-wind diffusion of the discontinuity.

4. In all cases the discontinuities spread out in the cross-wind direction. As all characteristics are parallel to the discontinuities nothing can counteract the above affect [N.B. the difference with shocks in test case 4].

5. PSI appears to be the best scheme, capturing the discontinuities both sharply and smoothly.

Non-linear Advection with Discontinuous Solution

The final test case looks at a non-linear Burgers'-type equation,

$$u_t + \left(\frac{\partial f}{\partial u}\right)_x + u_y = 0$$

over the domain $(x, y) \in [0, 1]$x$[0, 1]$.

Using the linearisation (4) gives a local cell velocity $\vec{\lambda} = (\bar{u}, 1)^T$ where $\bar{u}$ is an average of the u-values at the cell vertices.

The initial conditions are $u = 1.5 - 2x$ throughout the domain, with boundary conditions

$$\begin{aligned} u(x,0) &= 1.5 - 2x \quad \text{for} \quad 0 \le x \le 1, \\ u(0,y) &= 1.5 \quad \text{for} \quad 0 \le y \le 1, \\ u(1,y) &= -0.5 \quad \text{for} \quad 0 \le y \le 1. \end{aligned}$$

This ensures the generation of an oblique shock as shown in the analytic solution depicted in Figure 17.

Figure 18 shows the steady state solutions of 5 schemes with a maximum (theoretical) CFL number of 0.58, whereas Figure 19 shows in more detail the efficiency of the schemes at modelling the shock by taking a cut through the solution at $y = 0.75$.

Looking at the results, the following observations can be made:

1. In the lower part of the domain before the shock is formed, all schemes produce good straight lines, including the N-scheme. The latter is a result of the solution being approximately linear here and the regular grid.

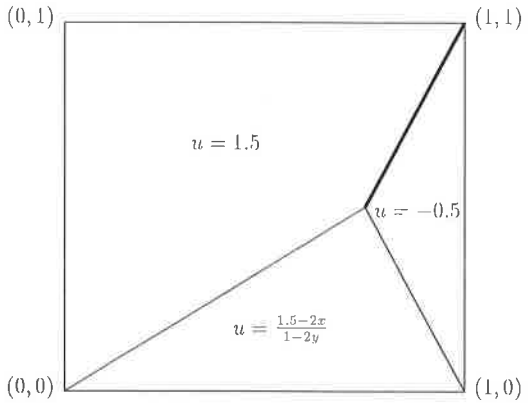

Figure 17: The analytic solution for the non-linear equation.

2. The shock is most sharply captured by the LP schemes.

3. Looking carefully at the shock, the actual grid cells can be identified. For the LP schemes the shock appears to have cell-width of 2.

4. Any cross-wind diffusion does not increase with distance from the shock's origin. This is due to the fact that a shock has converging characteristics, thus cancelling out any numerical cross-diffusion. This 'self-sharpening mechanism' of shocks [21] is not the same for contact discontinuities where the characteristics are parallel to it. [c.f.:- behaviour of the discontinuity in the last case].

3 Fluctuation Distribution Schemes on 2D Quadrilateral Grids

As mentioned earlier, fluctuation distribution schemes on triangular grids have been widely investigated and are believed to have reached a level of maturity. Obviously, they have received the greater attention due to their greater geometric flexibility in solving real-life problems. However, it has been noticed in [22] that quadrilateral grids produce more accurate solutions, more economically in areas such as stretched layers.

This has been the inspiration behind extending the fluctuation distribution schemes onto quadrilateral grids. Using approaches as with the triangle cases, equivalent schemes have been devised. The schemes to be reviewed apply for all quadrilaterals, as the previous section did for all triangles. However, the numerical results presented are derived using square cells.

As can be seen, this leads to a scheme producing nodal approximations at the same positions as using a triangular mesh. This gives us a medium in which to compare the performance of

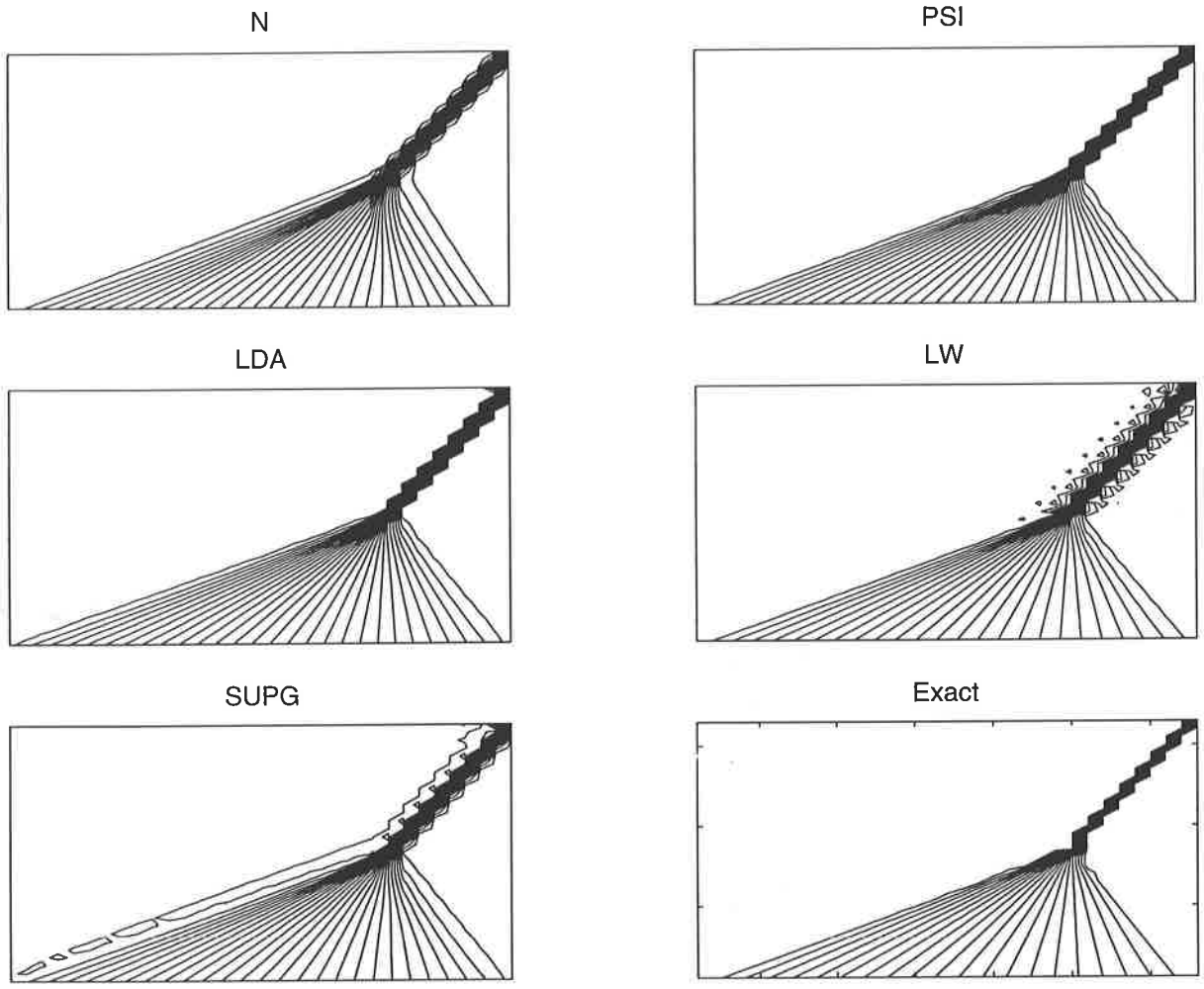

Figure 18: Schemes effectivity at shock capturing.

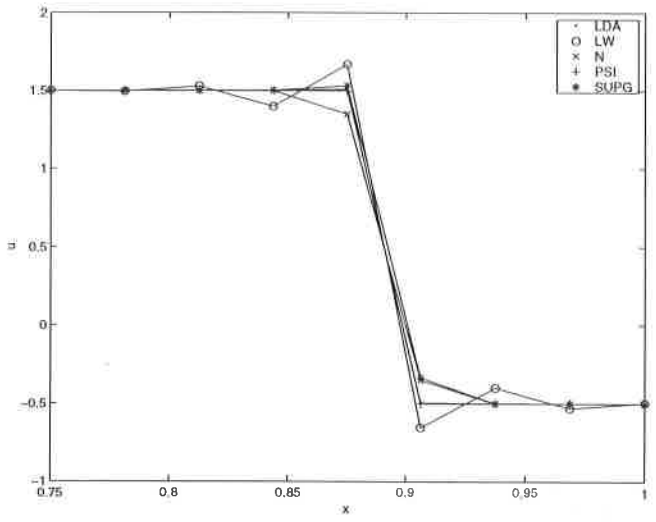

Figure 19: A cross-section through the oblique shock at y=0.75.

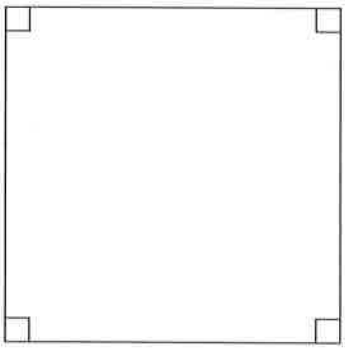

Figure 20: A square cell as used in this section.

the schemes and investigate the claim of Struijs and Deconinck,

> *'Freedom to cut the squares along either diagonal greatly enhances the performance of the schemes.'* [23]

Take an arbitrary quadrilateral, Q, in isolation, with vertices $v_1, ..., v_4$, edges $E_1, ..., E_4$ and scaled normals to the edges $n_1, ..., n_4$, labelled, as in Figure 21.

As before, the cell's fluctuation is defined by

$$\phi_Q = \oint_{\partial\square} u\vec{\lambda}.d\vec{n}$$

Once more, if u is assumed to vary linearly across the cell, then using the trapezium rule yields

$$\phi_Q = \frac{1}{2}(k_1 + k_4)(u_1 - u_3) + \frac{1}{2}(k_1 + k_2)(u_2 - u_4) \tag{18}$$

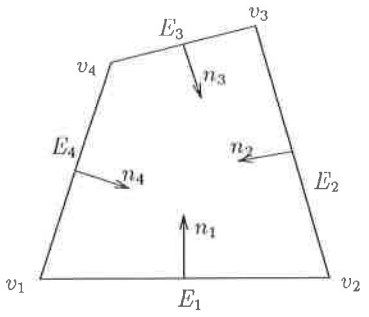

Figure 21: Labelling of a typical quadrilateral.

where $k_i = \frac{1}{2}\vec{\lambda}.\vec{n}_i$

Note, the extra rigidity bought about using the quadrilateral cells leads to natural comparisons being made with FE and bi-linear basis functions. This is further emphasised with the bilinear fluctuation distribution scheme [2].

The concepts of fluctuation distribution and conservation naturally move onto the new cells, as does the flow direction's relation to the $k_i's$. However, the concept of upwinding is not as obvious as before, as shall be seen.

The schemes have form

$$u_i^{n+1} = u_i^n + \frac{\triangle t}{S_i}\sum_Q \alpha_{T,i}\phi_T$$

and we desire the previously defined criteria of Continuity, Positivity and Linear Preservation.

3.1 Upwind Schemes

Upwind fluctuation distribution schemes only send fluctuation to downstream nodes. So, for downstream nodes i,

$$\alpha_{Q,i} = 0$$

Take the quadrilateral in Figure 21. Now, v_1 and v_3 are the upstream and downstream nodes respectively. However, the classification of v_2 and v_4 is less clear and is scheme dependent.

3.1.1 Linear Schemes

In this category there are two important positive schemes and one linearity preserving one. The first is the fluctuation distribution version of the simple first order dimensionally-split upwind scheme (the DS Scheme). The second is the quadrilateral version of the N scheme, the

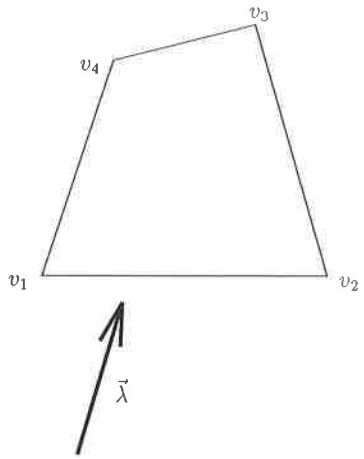

Figure 22: Flow into a quadrilateral.

optimal NQ Scheme. Finally there is the LDQ scheme, a second order accurate version of the LDA Scheme on quadrilaterals.

The DS Scheme

The positive first order DS Scheme uses the advection velocity approximated in the grid directions. It is a three target scheme, selecting the downstream nodes depending on the signs of $k_A = \vec{\lambda}.\vec{n}_A$ and $k_B = \vec{\lambda}.\vec{n}_B$ (see Table 3). Where $\vec{n}_A = \frac{1}{2}(\vec{n}_1 - \vec{n}_3)$ and $\vec{n}_B = \frac{1}{2}(\vec{n}_4 - \vec{n}_2)$ can be geometrically represented (see Figure 23). For the first case in Table 3, the distribution

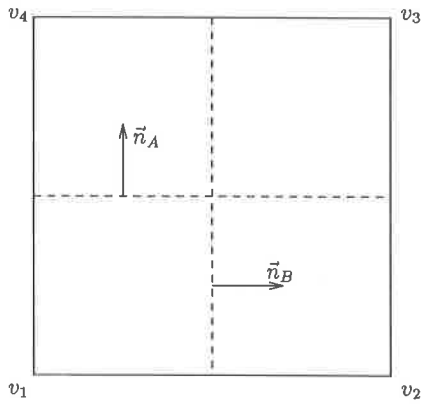

Figure 23: The geometric interpretation of $\vec{n}_A$ and $\vec{n}_B$.

coefficients are

$$\alpha_1 \phi = 0,$$

	Target
$k_A \geq 0, k_B \geq 0$	v_2, v_3, v_3
$k_A \geq 0, k_B \leq 0$	v_1, v_3, v_4
$k_A \leq 0, k_B \geq 0$	v_1, v_2, v_3
$k_A \leq 0, k_B \leq 0$	v_1, v_2, v_4

Table 3: Target nodes for the DS Scheme.

$$\begin{aligned}
\alpha_2\phi &= \frac{1}{2}\vec{\lambda}.\vec{n}_B(u_1 - u_2), \\
\alpha_3\phi &= \frac{1}{2}\vec{\lambda}.\vec{n}_A(u_2 - u_3) + \frac{1}{2}\vec{\lambda}.\vec{n}_B(u_4 - u_3), \\
\alpha_4\phi &= \frac{1}{2}\vec{\lambda}.\vec{n}_A(u_1 - u_4),
\end{aligned} \tag{19}$$

with the other cases obtained by simple cyclic permutations of the vertices.

The NQ Scheme

The NQ scheme [22] is the optimal first order scheme with respect to minimising cross-wind diffusion and so is the quadrilateral equivalent to the N-scheme. In fact numerical evidence in [2] shows the NQ scheme to outperform the DS scheme by a factor of 93 in terms of computational cost. It retains the exact advection direction unlike the DS scheme, and produces a two target scheme, dependent on the signs of $\vec{\lambda}.(\vec{n}_1 + \vec{n}_2) = k_1 + k_2$ and $\vec{\lambda}.(\vec{n}_1 + \vec{n}_4) = k_1 + k_4$, as in Table 4.

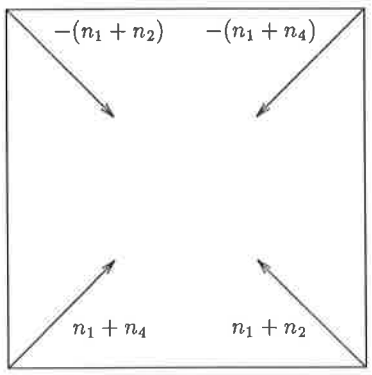

Figure 24: The directions used to define up/downstream nodes.

	Target
$k_1 + k_2 \leq 0, k_1 + k_4 \leq 0$	v_1, v_2
$k_1 + k_2 \leq 0, k_1 + k_4 \geq 0$	v_2, v_3
$k_1 + k_2 \geq 0, k_1 + k_4 \geq 0$	v_3, v_4
$k_1 + k_2 \geq 0, k_1 + k_4 \leq 0$	v_4, v_1

Table 4: Target nodes for the NQ Scheme.

Note: the distribution coefficients ensure that when the advection velocity is aligned with the diagonals $\vec{n}_1 + \vec{n}_2$ or $\vec{n}_1 + \vec{n}_4$ the scheme becomes one-target.

Taking the case where the targets are v_3 and v_4, the distribution coefficients are,

$$\begin{aligned}
\alpha_1\phi &= \alpha_2\phi = 0, \\
\alpha_3\phi &= \{k_1 + \min(0, k_2) + \min(0, k_4)\}(u_2 - u_3) + \{\max(0, k_4) - \min(0, k_2)\}(u_1 - u_3), \\
\alpha_4\phi &= \{k_1 + \min(0, k_2) + \min(0, k_4)\}(u_1 - u_4) + \{\max(0, k_2) - \min(0, k_4)\}(u_2 - u_4).
\end{aligned} \tag{20}$$

The other cases can be obtained with a cyclic permutation of the vertices. This is again a positive scheme but not LP.

The LDQ Scheme

The Low-Diffusion on Quadrilaterals Scheme (LDQ) is a linear, LP scheme, developed by Powell and Van Leer [24] using an area approach equivalent to that of the LDA scheme. Like the NQ scheme it is a two target scheme and selects these targets in the same way, although this is done automatically by the distribution coefficients,

$$\begin{aligned}
\alpha_1 &= \frac{\max\{0, -\vec{\lambda}.(\vec{n}_1 + \vec{n}_4)\}}{|\vec{\lambda}.(\vec{n}_1 + \vec{n}_4)| + |\vec{\lambda}.(\vec{n}_1 + \vec{n}_2)|}, \qquad \alpha_2 = \frac{\max\{0, -\vec{\lambda}.(\vec{n}_1 + \vec{n}_2)\}}{|\vec{\lambda}.(\vec{n}_1 + \vec{n}_4)| + |\vec{\lambda}.(\vec{n}_1 + \vec{n}_2)|}, \\
\alpha_3 &= \frac{\max\{0, \vec{\lambda}.(\vec{n}_1 + \vec{n}_4)\}}{|\vec{\lambda}.(\vec{n}_1 + \vec{n}_4)| + |\vec{\lambda}.(\vec{n}_1 + \vec{n}_2)|}, \qquad \alpha_4 = \frac{\max\{0, \vec{\lambda}.(\vec{n}_1 + \vec{n}_2)\}}{|\vec{\lambda}.(\vec{n}_1 + \vec{n}_4)| + |\vec{\lambda}.(\vec{n}_1 + \vec{n}_2)|}.
\end{aligned} \tag{21}$$

Again, this scheme reduces to having a single target under the conditions above.

3.1.2 Non-linear Schemes

Schemes such as the PSI scheme in the previous chapter are motivated by Sidilkover's observation (see [12]) that LP schemes can be obtained from P schemes with the use of a limiter. Mirroring the PSI derivation the MinMod function is used producing the NDS and NNQ schemes from the DS and NQ schemes respectively.

The NNQ Scheme

The non-linear, P, LP, NNQ scheme is obtained by supposing the two downstream nodes as defined for the NQ scheme receive contributions $\phi_1^\star$,$\phi_2^\star$,

$$\begin{aligned} \phi_1^\star &= \phi_1 - L(\phi_1, -\phi_2) \\ \phi_2^\star &= \phi_2 - L(\phi_2, -\phi_1) \end{aligned}$$

where ϕ_1 = contribution to node 1 from NQ scheme,
ϕ_2 = contribution to node 2 from NQ scheme,
L is the MinMod limiter (10).

3.2 The Lax-Wendroff Scheme

Using a stencil of the form of Figure 25, and the same approach as before the second order,

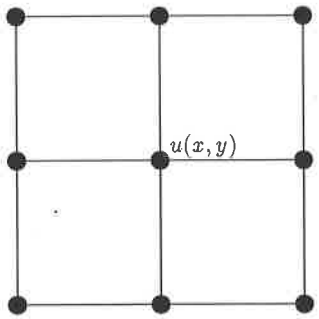

Figure 25: Stencil on quadrilaterals.

linear, LP, Finite Volume LW scheme is derived [25]. In fluctuation distribution form, it has coefficients

$$\begin{aligned} \alpha_1 &= \frac{1}{2}\{1 - \frac{\delta t_c}{V_c}[\vec{\lambda}.(\vec{n}_1 + \vec{n}_4)]\}, \qquad \alpha_2 = \frac{1}{2}\{1 - \frac{\delta t_c}{V_c}[\vec{\lambda}.(\vec{n}_1 + \vec{n}_2)]\}, \\ \alpha_3 &= \frac{1}{2}\{1 + \frac{\delta t_c}{V_c}[\vec{\lambda}.(\vec{n}_1 + \vec{n}_4)]\}, \qquad \alpha_4 = \frac{1}{2}\{1 + \frac{\delta t_c}{V_c}[\vec{\lambda}.(\vec{n}_1 + \vec{n}_2)]\}, \end{aligned} \tag{22}$$

where

$$\frac{\delta t_c}{V_c} = \frac{1}{|\vec{\lambda}.(\vec{n}_1 + \vec{n}_4)| + |\vec{\lambda}.(\vec{n}_1 + \vec{n}_2)|}.$$

Again, lacking in positivity, oscillations look to be a problem, especially near discontinuities.

3.3 Numerical Results

The performances of these new schemes are examined and compared to those of the triangle-based schemes on two of the test cases introduced in the previous section. The solutions are computed over a regular square grid with nodal spacing h=1/32 in both spatial directions. Firstly the time-dependent periodical linear advection of the double sine wave is investigated, followed by a look at contact discontinuities with the circular advection of the square wave.

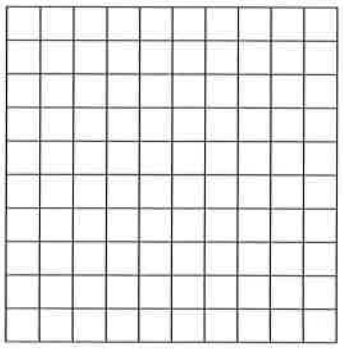

Figure 26: The grid used for the quadrilateral schemes.

Constant Linear Advection

The first case is the advection of the double sine wave (15). Figure 27 shows three of the quadrilateral schemes being compared to the equivalent schemes on triangles at t=1.0 for CFL=0.72. In the LDA case, where it has already been shown that Grid C produces superior results, this grid is used, whilst Grid A is used for the PSI and LW schemes. The performance of the NQ and DS schemes are investigated further in the next chapter, although mention of them is made in this section. Table 5 shows the numerical orders of accuracy of these five new schemes for this problem. From the given results the following observations can be made:

- The LDQ scheme suffers from streamwise diffusion and produces very similar visual results and order of accuracy as the LDA scheme on Grid A. The LDA scheme on Grid C as mentioned before, virtually eliminates this diffusion and holds the problems shape very effectively.

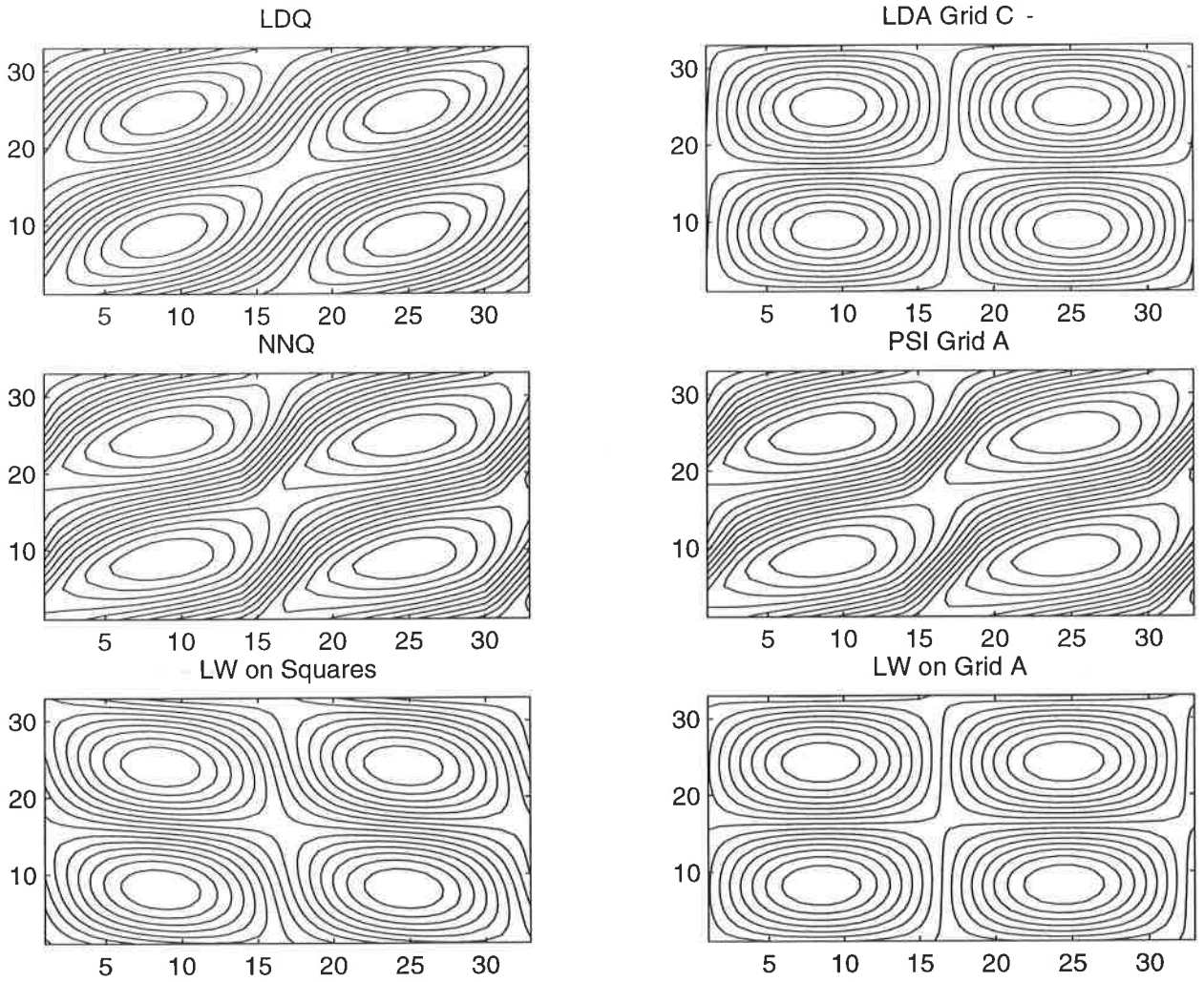

Figure 27: Advection of the double sine wave.

- The NQ scheme gives identical errors, hence an identical solution to the N scheme on Grid A. This is further investigated in the next chapter.
- The NNQ and PSI scheme on Grid A produce very similar results to each other, and relatively close to the N scheme on Grid A. In the last chapter it was said that the problem limiter was not used extensively in this problem, explaining the closeness of the results to their repective underlying schemes.
- As well as the customary phase lag, the LW on squares suffers from the curves diffusing into each other, and its inferior order of accuracy points to the triangular based solution being considerably better.

Scheme	L_1	L_{inf}
LDQ	0.83	0.85
LW	1.11	1.14
DS	0.73	0.75
NQ	0.78	0.82
NNQ	0.76	0.82

Table 5: Numerical orders of accuracy in the double sine advection case.

Circular Advection of a Discontinuous Solution

The second problem is the rotation of a square wave about the origin (17). Figure 28 shows the five square based schemes steady state solutions with a maximum CFL number of 0.45. Comparing the results with them of Figure (11) the following observations can be made:

- The NQ scheme (surprisingly maybe) is less diffusive than the N scheme, which in turn is less diffusive than the DS scheme. In fact, the N scheme seems to produce a solution which is 'between' the NQ and DS scheme.
- The LDQ and LW scheme both produce the expected oscillations near the discontinuities.
- The NNQ scheme is the most effective scheme seen so far on this problem, mapping the discontinuous part sharply and maintaining the smoothness of the rest of the solution.

So, does the above support Struijs and Deconinck's claim [24]. On the basis of the first problem the LDA and LW (triangles) schemes are superior, and the others relatively similar. When the velocity is non-constant (Problem 2), then the triangular grid based schemes start to develop problems. The next chapter attempts to look into these problems.

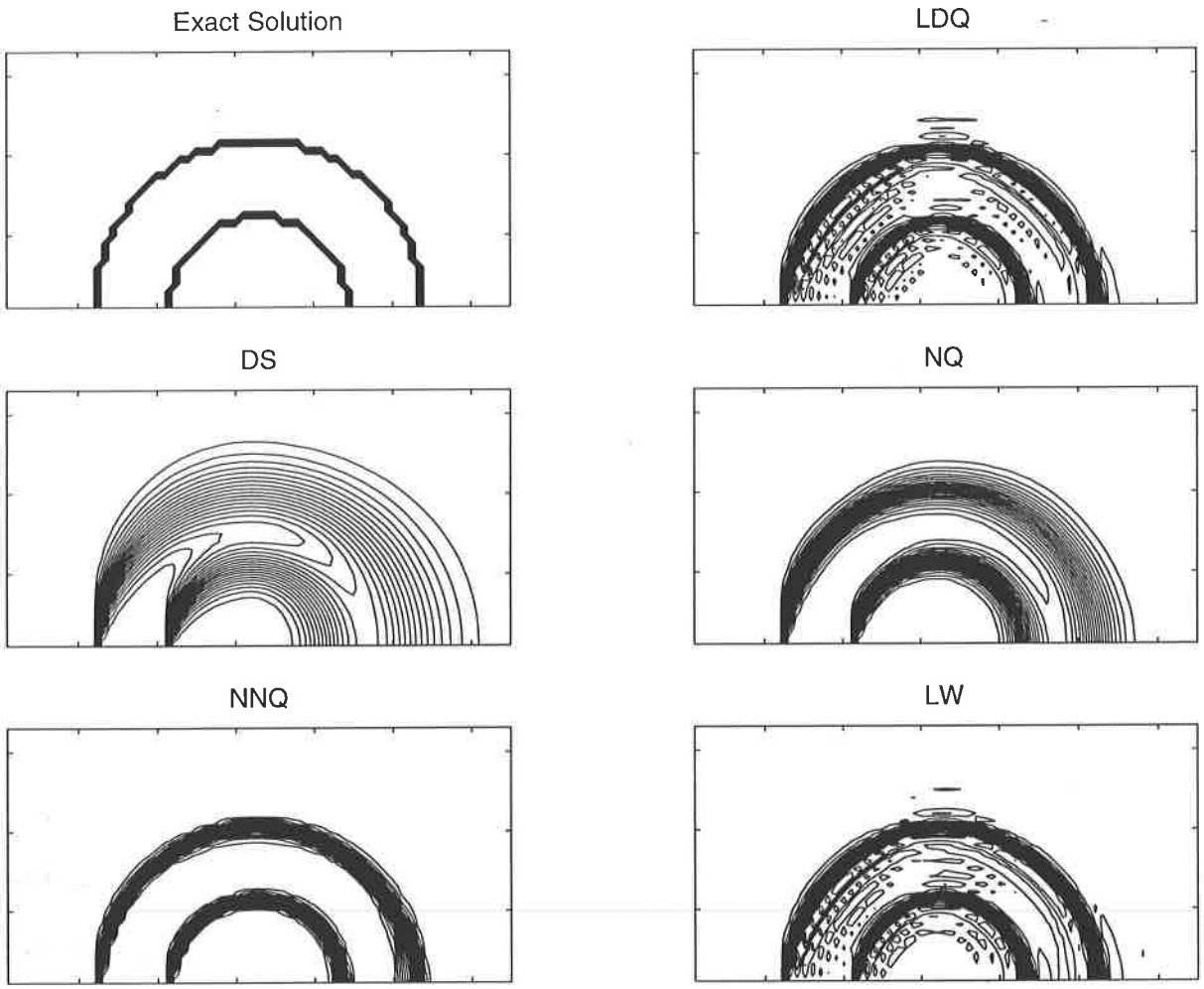

Figure 28: Advection of the double sine wave on Grid S.

4 Grid Adaption

One recoignised, and widely used way of improving numerical solutions to a problem is not to choose a better scheme, but rather to change the grid on which the scheme is working. Whether this be to create an initial grid appropriate to the problem and keep with it, or to alter the grid at every time-step as is often the case in the non-linear case, giving a solution dependent grid.

All schemes possess preferred grids and it would be the job of the analyst to search for its theoretical 'optimal' grid and construct a grid as close to this as possible. This can be achieved by either adding more nodes, altering the positioning/connectivity of the nodes already present, or some combination of the two.

In Chapter 2 a very simple example of mesh adaption was met. The nodes are neither

moved nor their numbers altered, but a simple change in connectivity to position the diagonals pointing the other way led to a considerable improvement in the performance of the LDA scheme. In this chapter, a similar phenomena is discovered concerning the N scheme via comparison with the NQ and DS schemes. It is seen how such a result paves the way for more extensive and complicated grid adaption.

4.1 Grid Adaption

The two main areas of adaptive mesh techniques are [26]:

- Grid Movement - a purely node movement technique, whereby the numbers of nodes stay fixed, but move around the grid.
- Grid Refinement - extra nodes are added to create a finer mesh in areas where the solution gradient is high e.g. discontinuities, shocks. Conversely nodes may be removed from areas of constant or slowly varying solutions.

Typically, some approximate technique is used to monitor the error, and the above techniques are employed in an attempt to reduce it. Obviously, the adapted grids are method-dependent, but usually result in grids with nodes clustered around shocks and discontinuities, not surprisingly so. But also, it can be seen that the cells themselves re-align themselves in an orientation dependent on the flow direction.

4.2 The N Scheme on a Quadrilateral Grid

The work in Appendix A is motivated by an observation of Roe [23]. It is shown that using the N Scheme on structured triangles with diagonals in the same direction as the advection yields a scheme equivalent to the NQ Scheme on the underlying quadrilateral grid. Likewise, using the N Scheme on triangles with diagonals in the opposite direction to the flow is equivalent to carrying out the DS Scheme on the underlying grid.

Looking at truncation error, the DQ Scheme has leading term

$$\frac{\Delta x}{2}|\sin\theta\cos\theta|\{|\sin\theta|+|\cos\theta|\}, \tag{23}$$

compared to that of the NQ Scheme,

$$\frac{\Delta x}{2}|\sin\theta\cos\theta|\{|\sin\theta-\cos\theta|\}, \tag{24}$$

which is, on average, four times smaller than (23).

It seems perfectly reasonable and sensible to thus select or adapt a grid dependent on the problem, hence maximising the scheme's potential.

It should be noted that since the limiting for the PSI scheme and the NNQ scheme occur with respect to different cells, the equivalence of the underlying schemes is not preserved for the limited versions. This explains the slight differences in their performances in the sine wave problem. For the rotating square wave, when x is positive, the velocity is travelling in the opposite direction to the diagonals, explaining the poor performance of the N scheme and subsequently the PSI scheme.

4.3 Improving Grids for Linear Advection

It is presumed that the θ above is an angle between the flow direction and the grid lines[3]. So, if grid lines could be orientated to point in the flow direction these leading terms would also vanish, thus giving the schemes an order of two. It is highly likely that all such coefficients in the truncation error possess the factor $|\sin\theta\cos\theta|$, and hence such a grid alignment would result in perfect advection of the solution. This suspicion is confirmed by advecting the sine wave with $\vec{\lambda} = (0,1)^T$, and $\vec{\lambda} = (1,0)^T$.

A similar phenomena can be observed for triangles. Applying a grid movement technique on a scheme suggested by Roe resulted in perfect advection for a grid in which each triangle had an edge alligned with the advection direction [27]. A scheme presented by Baines, Leary and Hubbard [28] possesses an optimal grid with cells aligned with the discontinuities and shocks of the problem.

For the N scheme the previous section tells us that a grid of type D (Figure 30) is preferable to a grid of type A. It is highly likely that the grid may be further improved by allowing cells to align with the discontinuity, i.e. where the scheme may have problems. Further evidence of this is given in [29] where an *Equidistribution Algorithm* is used to generate an optimal grid with respect to error, for the PSI scheme on the rotating square wave problem (See Figure 29).

4.4 Numerical Results

Numerical evidence of the effect of swapping diagonals is shown with the help of a new type of grid (see Figure 30), especially formulated for the problem of circular rotation. Two problems are chosen in order to see the respective diffusions caused by this and grids already met, for the same schemes. Firstly the linear advection of the sine wave is used, followed by the introduction of a new test problem - the circular rotation of a cone.

[3]Roe does not mention its origin, but subsequent work and consultation with Prof. Mike Baines makes this the most likely option.

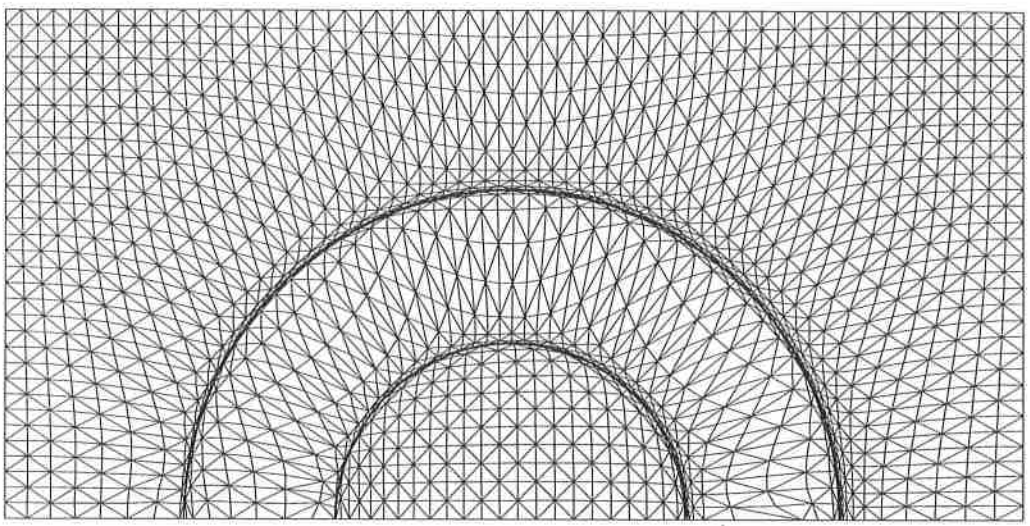

Figure 29: The optimal grid for the PSI scheme and rotating cone (Hubbard)

Constant Linear Advection

The first test case is the advection of the sine wave (15). Figure 31 shows the equivalence of the NQ and DS schemes to the N scheme for diagonals in the same and opposite direction to the flow respectively, on such structured grids. Using this equivalence, the results from Table 5 show that the N scheme's order of accuracy is approximately 0.05 greater on grid A. Looking at the plots, it can be seen how diffusion takes place in the direction of the diagonals. Stream-wise for grid A and cross-wise for grid C.

Circular Advection

The second test case models the rotation of a cone 360° about the origin with velocity $\vec{\lambda} = (\pi y, -\pi x)^T$, in the domain $(x, y) \in [-1, 1]$x$[0, 1]$. The initial conditions are:

$$\begin{aligned} u(r) &= \cos^2 2\pi r \qquad \text{for} \qquad r \leq 0.25, \\ u(r) &= 0 \qquad\qquad\quad \text{elsewhere,} \end{aligned} \tag{25}$$

where $r^2 = (x+0.5)^2+y^2$. In a similar manner to the sine curve, after t=2.0 the solution should have completely rotated and be back in its initial position. So the results can be compared to the initial solution (see Figure 32). Due to stability problems on Grid A the problem was

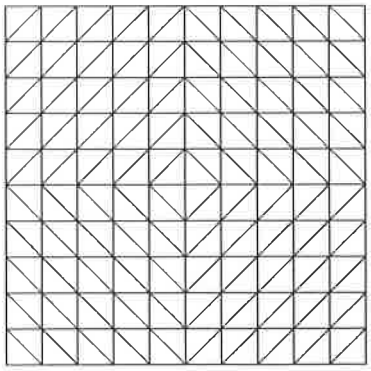

Grid D

Figure 30: Grid constructed for circular advection.

carried out at a low CFL number, maximum 0.23. Figures 33 and 34 show the solution after one rotation using the N scheme on Grids A and D. The contour plots show extra diffusion on Grid A, especially in the streamwise direction, whilst the side-on plot shows the peak of the cone has decreased far more on Grid A. Remembering that the N scheme is more effective when the characteristics are in the same directions as the diagonals, this can be explained by the fact this is always true for Grid D but only true in the upper left and lower right quadrants for Grid A, i.e. a grid to fit the problem has been created.

5 Scheme Improvements

In the preceding chapters, it has been seen that the higher order schemes such as SUPG and LW suffer from non-monotonic solutions, generating spurious oscillations, most notably in the vicinity of discontinuities. In fact, it is well known that linear schemes cannot be both second order and positive (Godunov's theorem).

In one-dimension, the term Total Variation Diminishing (TVD) was introduced by Harten [20] as a sufficient condition for a scheme to impose monotonicity. TVD can be achieved with the use of either Flux or Slope Limiting schemes. The former family of scheme (used as post-processors) involves the creation, then modification of the solution, and amongst them is the Flux-Corrected Transport (FCT) Scheme proposed by Boris and Book [6], [7] in one-dimension.

Generalised into two-dimensions by Zalesak [8], it is a two-staged algorithm involving the use of a higher order non-monotone scheme combined with a monotone lower order scheme to create as higher order scheme as possible which does not create new extrema.

Another problem with the fluctuation distribution schemes is that of accuracy in time. For the schemes first devised in a fluctuation distribution format, e.g. LDA, N, simple Euler

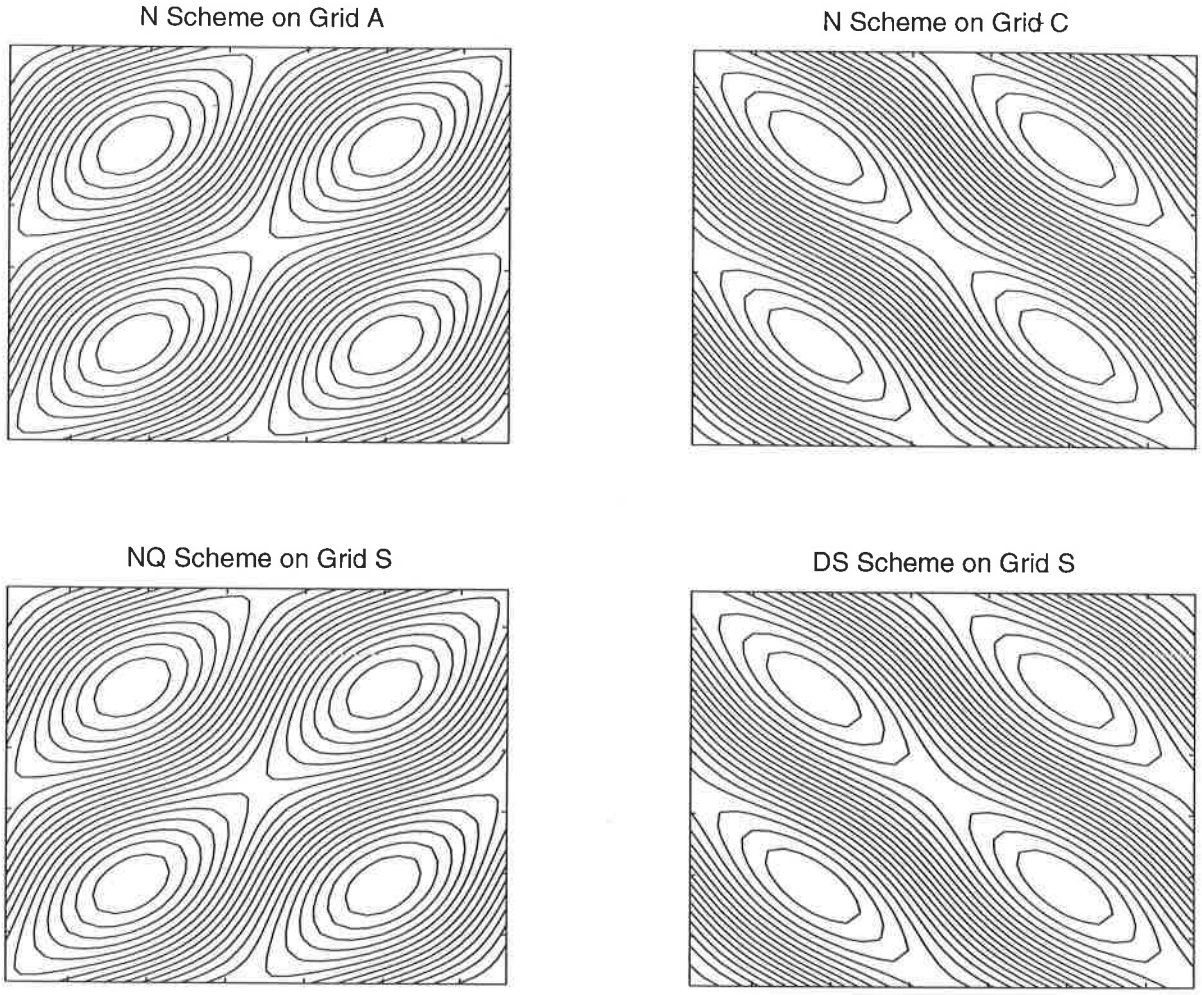

Figure 31: Advection of the sine curve.

time-stepping is employed. First order accurate in time, this has no effect on the steady state problems where artificial 'psuedo' time-stepping is employed. However, when time-dependent problems like the advecting sine-curve or rotating cone are investigated this limits the overall accuracy of the scheme. Those schemes with other origins such as LW and SUPG gain higher order time accuracy by having the distribution coefficients as functions of the time-step, ΔT.

The FCT algorithm attempts to do this by resorting to the higher order LW scheme whenever possible, and März [5] succeeds to some degree by taking a Petrov-Galerkin type, FE approach, creating a consistent mass matrix. In this project an attempt is made to improve time accuracy by replacing the Euler time-stepping with the TVD Runge-Kutta (RK) time discretisation used by Shu and Osher [21] in the hope that the overall order of accuracy is no longer time-step dependent, and thus reaches an order close to that of a steady-state problem.

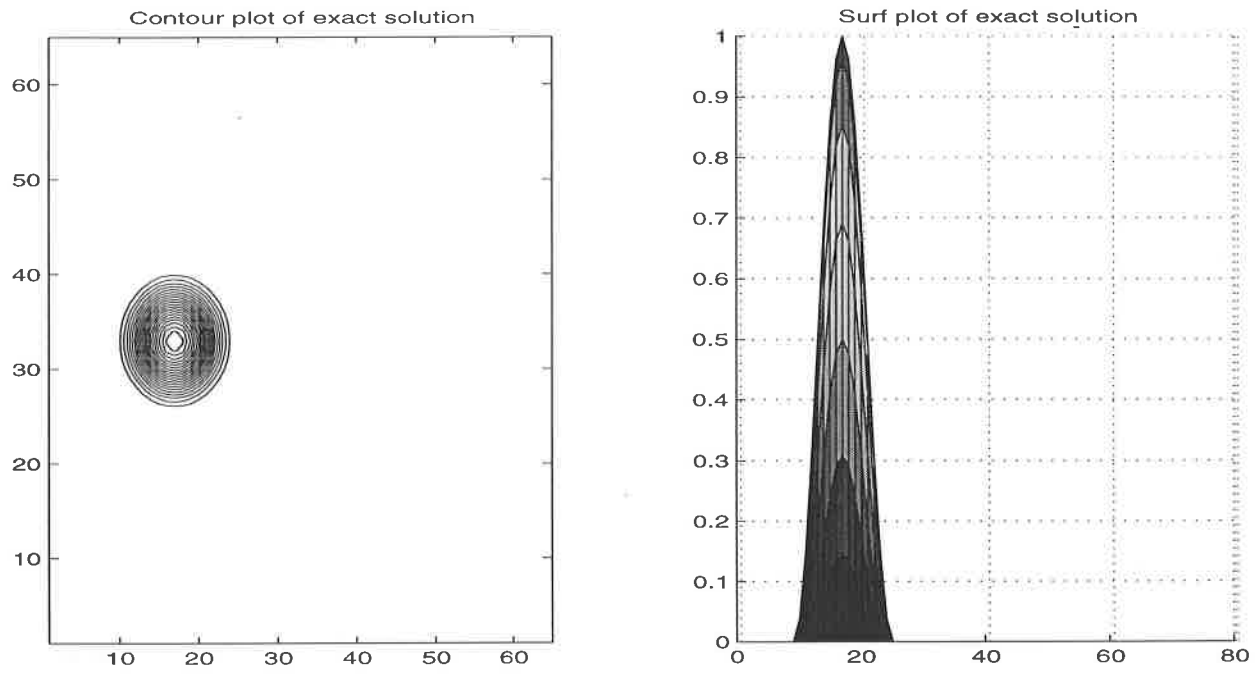

Figure 32: The initial solution for the rotating cone problem.

5.1 The FCT Algorithm

The FCT algorithm involves using a combination of a higher order non-monotone scheme (typically LW) and a lower order monotone scheme (typically PSI) in such a manner that the higher order method is used to the greatest extent possible without producing new extrema at the next time-level. Consequently, this results in the higher order scheme dominating in smooth regions and the lower order scheme being favoured for a locally rapidly altering solution.

Using notation from [9], the scheme can be written as:

1. For each triangle, j:

   (a) Compute the Lower Order Element Contributions to nodes i (LEC_i^j) for the PSI scheme.

   (b) Compute the Higher Order Element Contributions to nodes i (HEC_i^j) for the LW scheme.

   (c) Compute the Antidiffusive Element Conributions (AEC_i^j), given by,

   $$\mathrm{AEC} = \mathrm{HEC} - \mathrm{LEC}.$$

2. Transport Step - for each node, i:

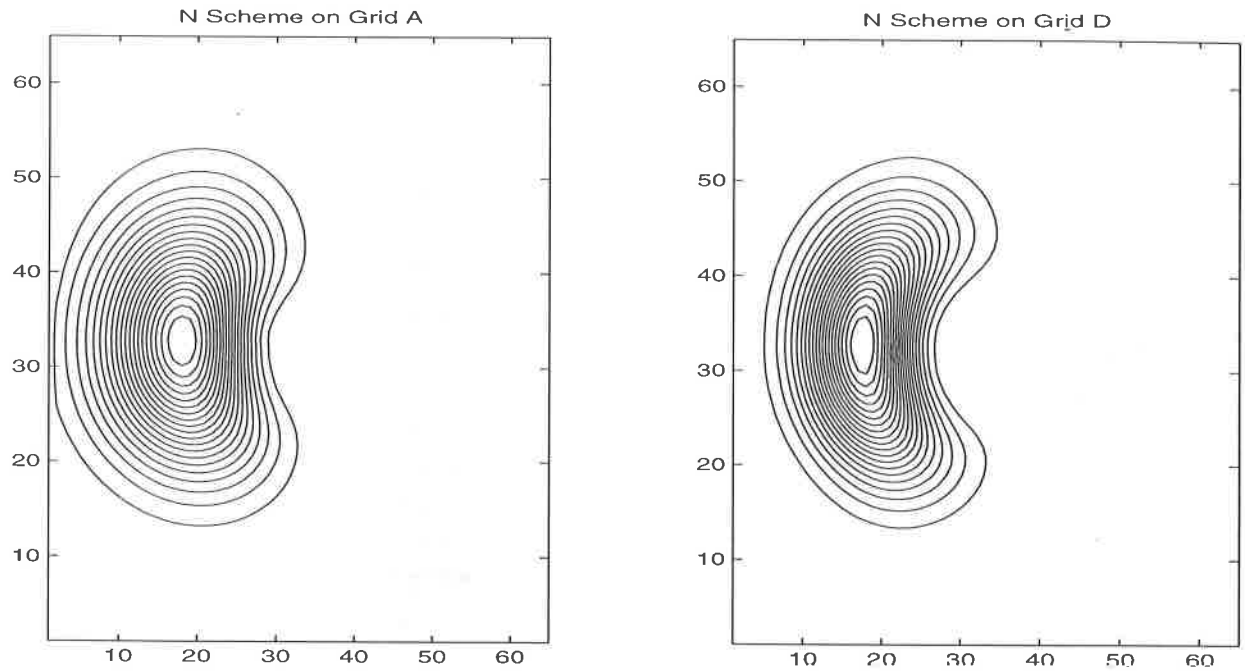

Figure 33: Contour plots of the solutions after one rotation.

- Compute a lower order update

$$u_i^L = u_i^n + \sum_{j \in \Delta_i} \mathrm{LEC}_i^j.$$

3. Limiting Step - for each $\triangle$:

   - Limit the Anti-Diffusive contributions such that,

$$\mathrm{AEC}_i^j = \beta^j \mathrm{AEC}_i^j \qquad , \qquad 0 \leq \beta^j \leq 1.$$

4. Corrector Step:

   - Compute the final solution,

$$u_i^{n+1} = u_i^L + \textstyle\sum_{j \in \cup \Delta_i} \mathrm{AEC}_i^j.$$

The limiting procedure required to find the β^j's in Step 3 is described in [8]. In the Fluctuation Redistribution Algorithm of [9] this is taken one stage further by using individual triangle/node limiters β_i^j. However, with this more flexible approach, extra care must be taken to ensure conservation, which is automatially ensured with the FCT approach.

5.2 Runge-Kutta Time-Stepping

Improving the order of accuracy of fluctuation distribution schemes has been attempted with some success in papers such as [5], where the PSI scheme has been seen to almost double in

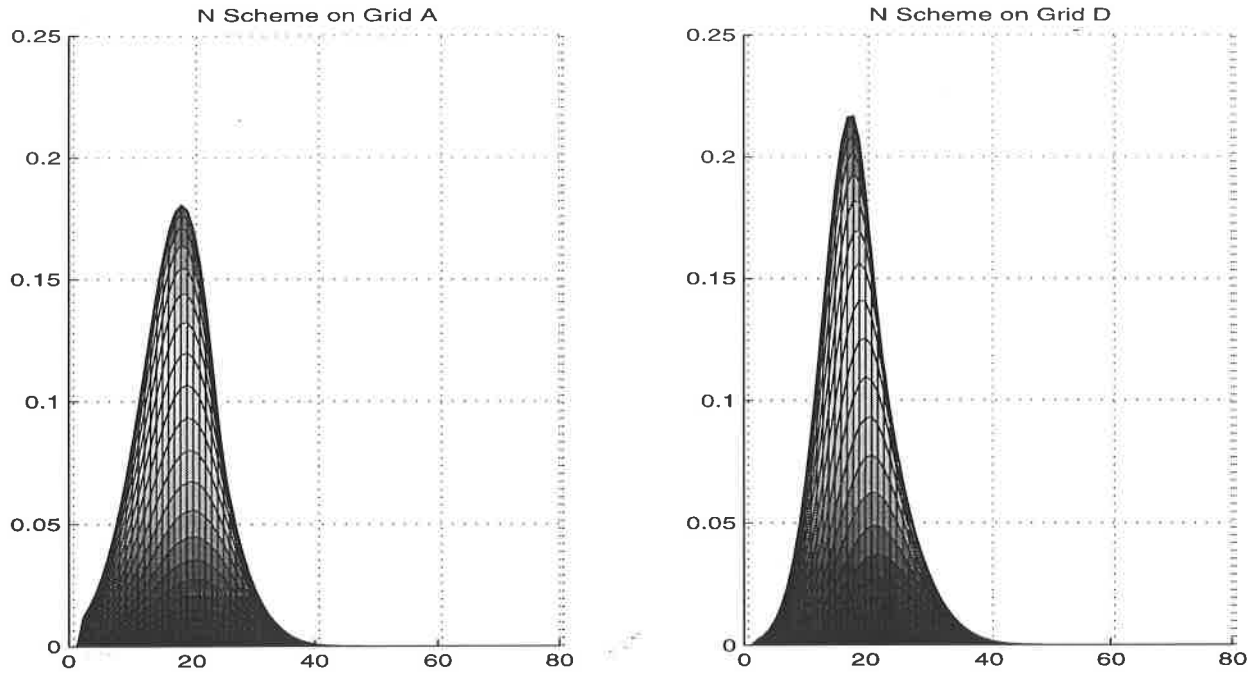

Figure 34: A side on plot of the solutions after one rotation.

accuracy for the advecting double sine wave case on Grid A [9]. Also Jameson manages to stabilise his central FV scheme with the use of RK time-stepping [17].

The following method is taken from work done in [21] to improve the time accuracy of the essentially non-oscillatory (ENO) slope-limiting TVD scheme. Previously ENO had used Euler time-stepping which is assumed to be TVD [21]. This is then replaced by an r-th order accurate RK time discretisation with coefficients chosen to ensure TVD, where r is the order of the spatial operator. It can be written as

$$u^{(i)} = \sum_{k=0}^{i-1} \alpha_{ik} u^{(k)} + \beta_{ik} \Delta T L(u^{(k)}) \qquad , \qquad i = 1, .., r.$$

where, $u^{(0)} = u^n$, $u^{(r)} = u^{n+1}$, and $L(u)$ is the scheme's spatial operator.
Now the coefficients for the methods are

Order	α_i	β_i
2	1	1
	$\frac{1}{2}$ $\frac{1}{2}$	0 $\frac{1}{2}$
3	1	1
	$\frac{3}{4}$ $\frac{1}{4}$	0 $\frac{1}{4}$
	$\frac{1}{3}$ 0 $\frac{2}{3}$	0 0 $\frac{2}{3}$

and so, the idea is to use RK time-stepping in the fluctuation distribution methods. Hence

the above scheme can be used, with

$$L(u) = \frac{1}{S_i} \sum_T \alpha_{T,i} \phi_T.$$

5.3 Numerical Results

The effectiveness of these two improvements is tried out on two of the test problems. Firstly, the advecting sine-wave is investigated, then the rotating square wave, to gauge the performance of these techniques a on selection of schemes.

Constant Linear Advection

The first case is the advection of the double sine-wave (15). Figure 35 shows the results after t=1.0 of using the FCT and Fluctuation Redistribution Algorithms with the PSI and LW schemes, against those of their underlying schemes. The test is done on a grid type A with CFL number 0.72. Both the FCT and Fluctuation Redistribution schemes give solutions very similar to the LW scheme, implying there is little need to resort to the lower order PSI scheme. This is further emphasized with the numerical orders of accuracy for this problem, giving L_1 orders of 1.99 for both schemes, and L_{inf} orders of 2.01 and 1.25 for the Fluctuation Redistribution and FCT Schemes, respectively. In fact looking at the actual errors, they are all very similar, most notably between the LW and Fluctuation Redistribution Schemes. However, the greater accuracy of the latter scheme over FCT does come at the price of a posible loss of conservation.

The problem was also tried using RK2 and RK3 time-stepping on the PSI and LDQ schemes. The results for refining the grid were practically identical for both RK2 and RK3, implying that it seems a waste to employ a time-stepping method of order greater than the spatial operator. The results for the grid refinement are shown in Figure 36. The numerical order of accuracy, is the asymptotic gradient with respect to Log(dx). Before, the curve had levelled out quickly, but in this case it is continuing to steepen despite considerable refinement. All that can be concluded from this graph is that, by observing the general trend, the order of accuracy is at least that of the most refined gradient 0.90 and 0.88 in the PSI case and 0.86 and 0.89 in the LDQ case for L_1 and L_{inf} orders respectively. The hope would be that as Log(dx) $\rightarrow -\infty$ that the gradients would approach 1.65 for PSI and 2.00 for LDQ, their steady state orders of accuracy. However, whether this happens or not, the RK2 time-stepping has still brought about an increase in accuracy over the Euler time-stepping.

Circular Advection of a Discontinuous Solution

The second problem is the square wave being rotated about the origin (17). Figure 37 shows

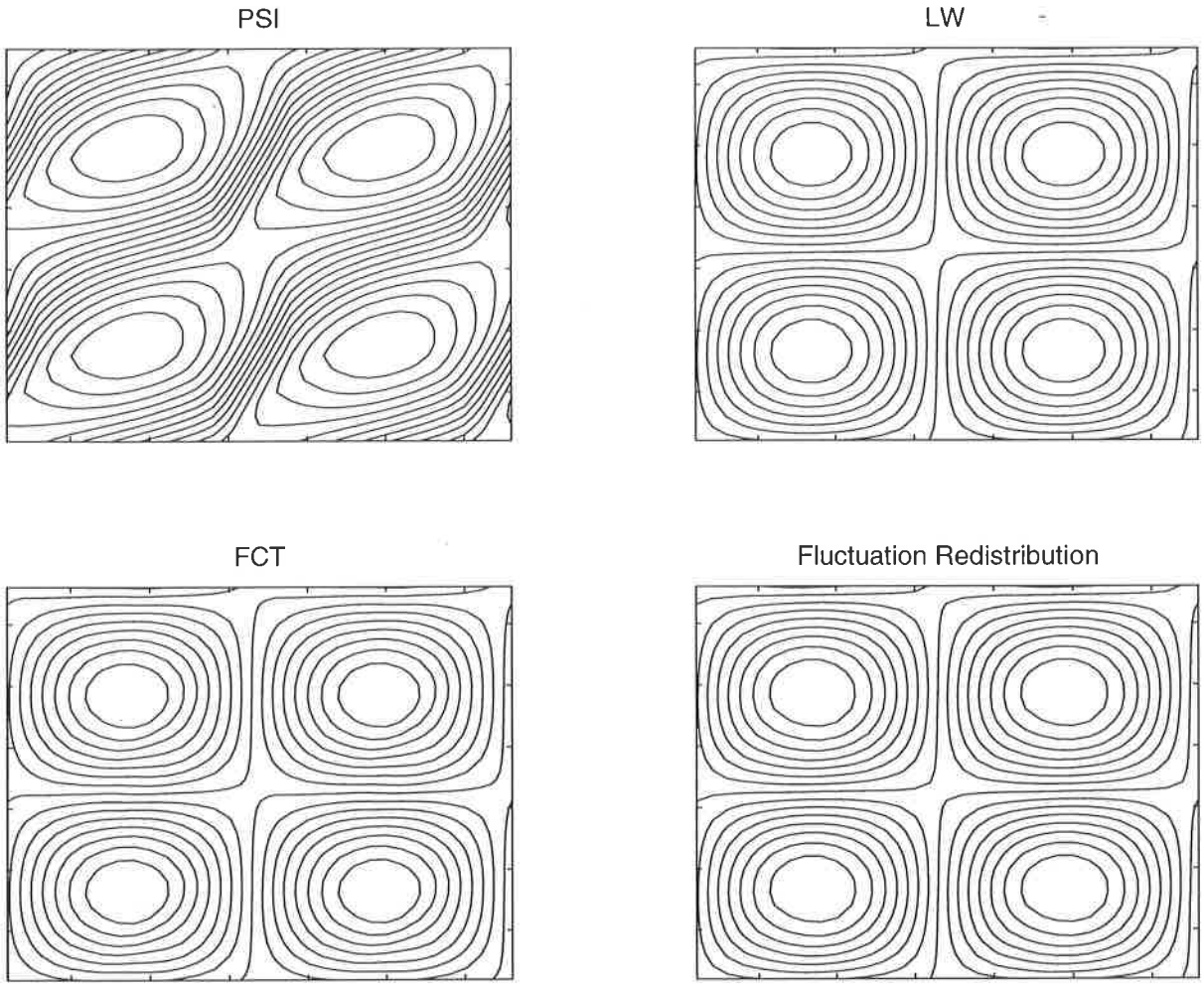

Figure 35: The advecting sine curve at t=1.0

the performance of the FCT and Fluctuation Redistribution Algorithms compared to their underlying schemes on Grid A with maximum CFL=0.45. As expected they model the discontinuity very sharply, nearly as well as LW, but do not suffer from the spurious oscillations which plague the LW solution. For the Fluctuation Redistribution case the solution does not seem to model the discontinuity quite as well, possible due to a lack of conservation.

6 A New Scheme

This chapter looks at a new, third order spatially accurate scheme which will simply be called the 3rd Order Scheme in this project. Derived in a similar way to the LW scheme it has been proposed by Hubbard (private communication). The scheme has been shown by the proposer to be unconditionally Fourier unstable, hence some of the techniques and ideas introduced in

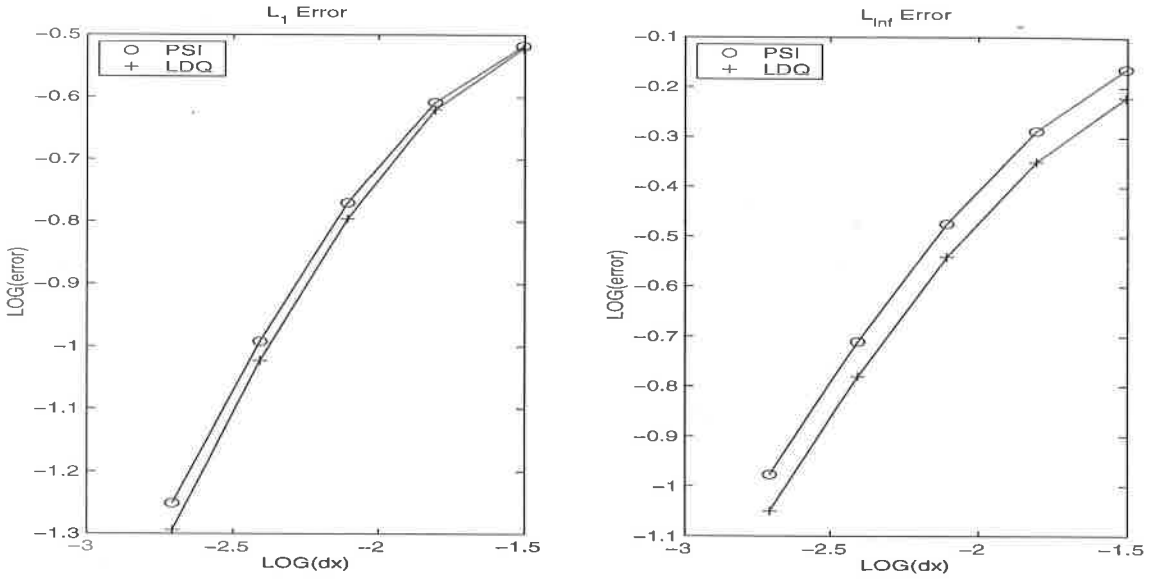

Figure 36: Numerical orders of accuracy using RK2 time-stepping on Grid A.

this project are used in an attempt to improve the scheme.

6.1 The Scheme

The idea behind Hubbard's new scheme is to take a Taylor Series, truncated to first order in time,

$$u^{n+1} \approx u^n + \triangle t u_t$$

as with Jameson's central scheme [17], and derive a scheme using the steps as for the LW scheme (see Section 2.2), but with two differences:

- In Step 4 the stencil used incorporates nodes on the next band of triangles out (see Figure 38).
- In Step 7 the coefficients are found to satisfy spatial accuracy up to order 3.

So the scheme uses a less compact stencil similar to those used by the slope limiting algorithms like ENO. This loss of compactness inevitably leads to longer computer run-time as well as a requirement for more storage.

Simple calculus shows that only ten degrees of freedom are needed to make the scheme third order accurate in space, whilst there are thirteen points in the stencil. Hence the proposer has a great deal more flexibility than Jameson and consequently refined his stencil to give it a more upwind nature. He accomplished this by getting rid of the furthest downstream nodes (see Figure 39).

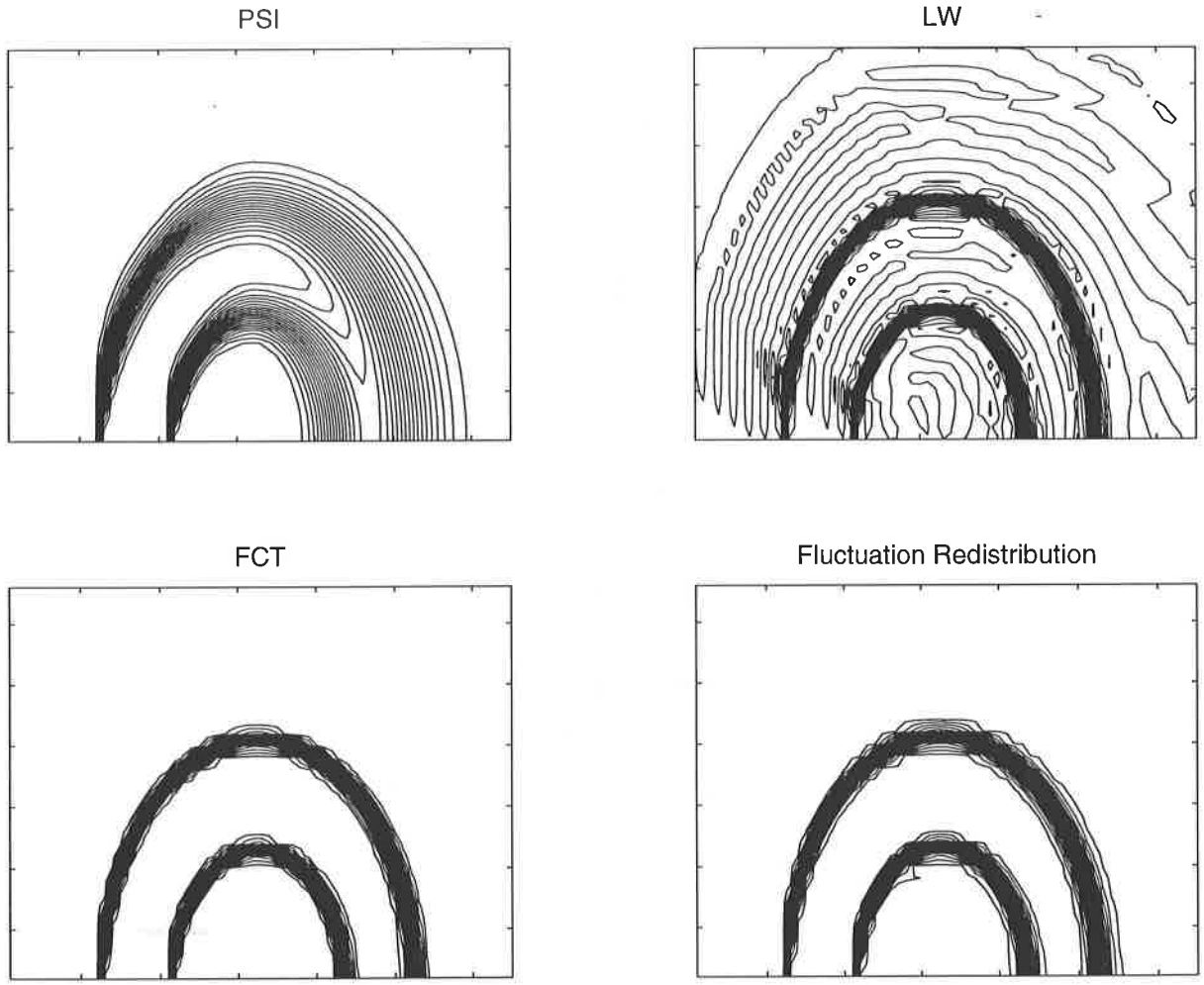

Figure 37: The rotating square wave at steady state.

The resultant scheme may be written in fluctuation distribution form, where the fluctuation is distributed to the nodes of neighbouring cells, as well as its own, as follows:

(I) If there is 1 inflow edge, then

- $\alpha_i^T = \frac{1}{3}$ where i are upstream vertices of T.
- $\alpha_i^T = 1$ where i is the downstream vertex of T.
- $\alpha_i^T = -\frac{1}{3}$ where i are vertices of opposite outflow edges.
- $\alpha_i^T = 0$ where i is the vertex opposite inflow edge.

(II) If there are 2 inflow edges, then

- $\alpha_i^T = \frac{2}{3}$ where i are downstream vertices of T.

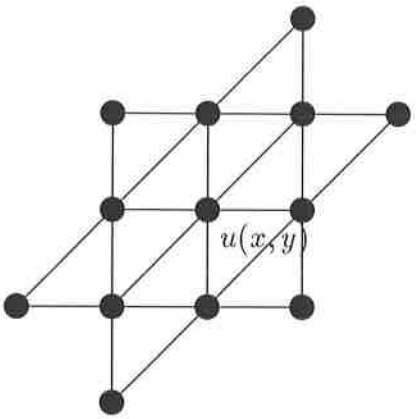

Figure 38: Extended stencil on a Type A grid.

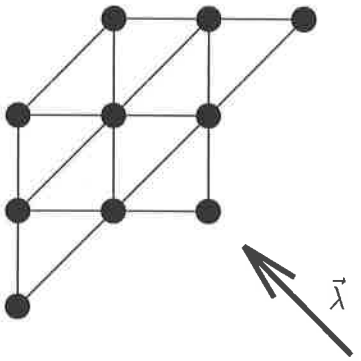

Figure 39: The refined upwind stencil on a Type A grid.

- $\alpha_i^T = -\frac{1}{3}$ where i is the vertex opposite the outflow edge.
- $\alpha_i^T = 0$ for all other vertices.

In both cases

$$\sum_{i=1}^{6} \alpha_i^T = 1,$$

hence the scheme is conservative.

Carrying out a standard Fourier stability test on the scheme shows that it is impossible to guarantee stability, and hence the solution may blow up. In an attempt to stabilise the method, 2 separate methods have been tried. Firstly the FCT algorithm is used to prevent the solution from growing, and secondly, the simple Euler time-stepping is replaced with a TVD RK3 approximation to the time derivative.

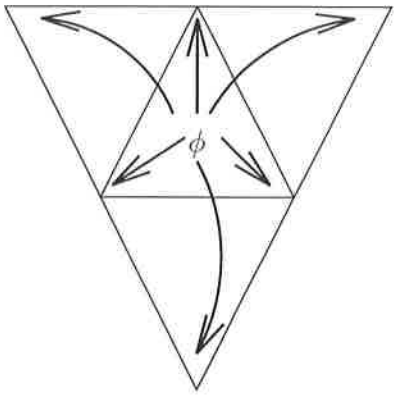

Figure 40: Distribution under the new scheme.

6.2 Grid Type

For the methods previously met, it has been shown that the orientation of the triangles diagonals can significantly affect the performance of the scheme. Having diagonals in the same direction as the flow will lead to streamwise diffusion and cross-wind diffusion for the diagonals facing the other way.

All schemes have natural diffusion in some direction. It is a case of weighing this up with the grid induced diffusion to produce the optimal combination. For the LDA Scheme, shown to have only streamwise diffusion, the grid was chosen which produced mainly cross-wind diffusion (Chapter 2). For the N Scheme, naturally producing both types of diffusion the grid producing mainly streamwise diffusion was preferred (Chapter 4). Will there be a similar dependence on grid type for this new method? The two stencils are shown in Figure 41.

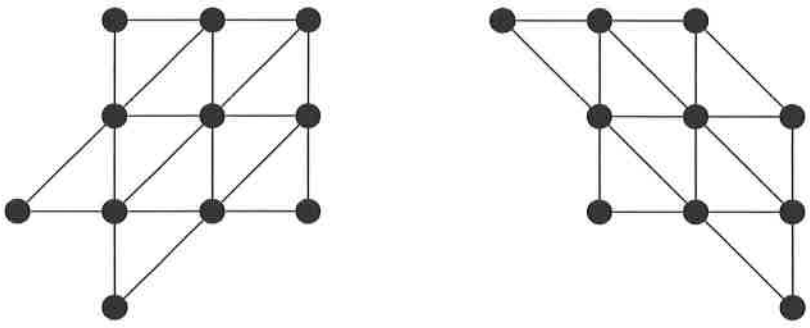

Diagonals in same direction as flow. Diagonals in opposite direction to flow.

Figure 41: Stencils for positive flow.

As before, it is obvious that the first stencil will produce streamwise and the second cross-wind diffusion. Section 6.4 tries to find the preferred grid for the advection of the double

sine-wave.

6.3 Scheme Improvements

In Chapter 5, two methods of scheme refinement were met: the FCT Algorithm to suppress non-linear instabilities, and RK time-stepping to improve accuracy in time. It is to be seen if any of these are effective in stabilising the new scheme.

6.3.1 The FCT Algorithm

In the preceding chapter, the PSI Scheme was used to stabilize the LW Scheme with use of an anti-diffusive term in the FCT Algorithm. Retaining the use of the PSI Scheme, the method may be modified to encorporate the 3rd Order Scheme. So in the language of Section 5.1,

$$AEC_i^j = TEC_i^j - LEC_i^j$$

where TEC_i^j are the 3rd order method contributions to node i from cell j, and continuing as before gives the TVD FCT3 Algorithm.

The reality of the FCT Algorithm is that in areas of low solution gradient, the 2nd order LW Scheme is used without creating new extrema. The new scheme is third order accurate in space, and hence will reach third order accuracy for steady state problems. So, for such problems it makes sense to take the cells which do not create extrema for the LW Scheme and add as much of the 3rd Order Scheme as possible via a further limiting and corrector step.

The FCT3ex Algorithm

1. Carry out the FCT Algorithm giving solution u_i^{FCT}.
2. For all $\triangle$'s s.t. $\beta^j = 1$,
   (a) Compute High-Order Corrector Element Contributions such that,
   $\mathrm{CEC}_i^j = \mathrm{TEC}_i^j$ - HEC_i^j.
   (b) Limit the CEC_i^j contributions such that no further extrema are met,
   $\mathrm{CEC}_i^j = \gamma^j\ \mathrm{CEC}_i^j \quad , \quad 0 \leq \gamma^j \leq 1.$
3. Update solution
   - $u_i^{n+1} = u_i^{\mathrm{FCT}} + \sum_{j \in \cup \triangle_i, \beta^j = 1} \mathrm{CEC}_i^j$.

This method, as it distributes all the fluctuation, remains conservative. The details of how to obtain the limiters γ^j may be found in Appendix B.

Grid	L_1	L_{inf}
A	1.25	1.19
C	1.62	1.63

Table 6: Numerical orders of accuracy for the 3rd Order Method.

Note: Since the 3rd Order Scheme is only first order accurate in time, its order of accuracy for time-dependent problems is probably below that of the LW Scheme (see Section 6.4). So, using the above on such a problem would result in increasing, then decreasing the accuracy. Therefore, the above will only be effective on steady-state problems.

6.3.2 RK3 Time-stepping

In order to create overall third order accuracy, an approximate time-derivative of at least order three should be used. In Chapter 5 it was seen that there is little point using a time-step of greater order than that of the spatial operator, so the RK3 method introduced in Section 5.2 is used.

6.4 Numerical Results

The effectiveness of the new scheme and its derivations was tried out on 2 test problems, firstly the advecting sine-wave, then the linear advection of a discontinuous solution.

Constant Linear Advection

The first problem is the case of the advecting double sine wave (15). Figure 42 shows the performance of the 3rd Order Scheme on Grids A and C, after t=1.0. The lower CFL number of 0.36 is required to prevent the solution completely blowing up, but even at this CFL number, the peaks have increased by around 75% (see Figure 43). Both grids lead to a 'stretching' of the solution in the cross-wind direction. Table 6 shows the numerical orders of accuracy for this problem, and implies that this method prefers a triangulation with the diagonals pointing in the opposite direction to the flow.

Figure 43 shows a cross-section through the sine-wave at $y = 0.25$ and t=1.0, for the basic 3rd Order and FCT3 Schemes. The analytic solution should be a standard sine-wave with max/min of +1/-1. As said before, the 3rd Order Scheme has caused the peaks to grow and troughs fall. The result of the FCT3 Algorithm is to 'squash' the solution into its analytic boundaries, leaving an inaccurate looking solution. In fact, the FCT3 Algorithm has order of

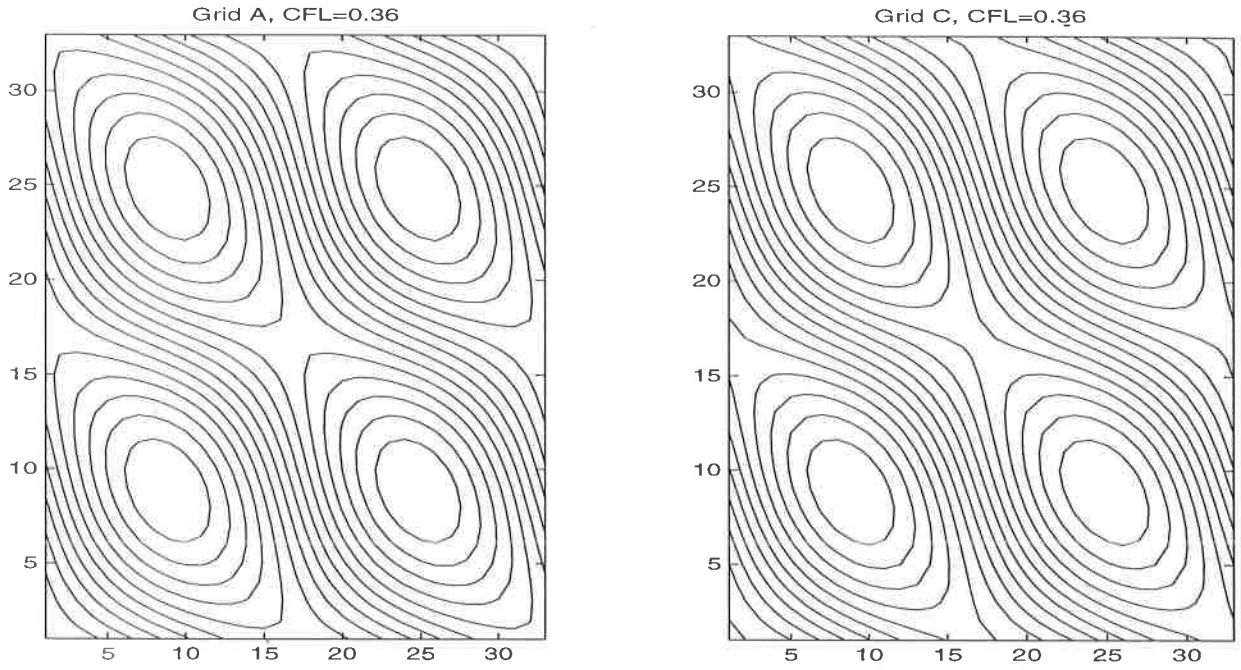

Figure 42: The Third Order Scheme on the advecting sine curve at t=1.0

L_1	L_{inf}
3.01	3.03

Table 7: Numerical orders of accuracy for the 3rd Order Scheme using RK3 on Grid A.

accuracy of less than one for this problem. Figure 44 shows far more pleasing results, from applying RK3 time-stepping on Grid A at CFL=0.72. The visual results show a stable solution with little distortion or diffusion. Grid refinement shows the third order accuracy has been reached (Table 7).

Constant Linear Advection of a Discontinuous Solution

The second problem is the mapping of a discontinous solution (16). Figure 45 shows the steady state solution on Grid A for CFL=0.32. RK3 time-stepping appears to have little or no effect here. This is of no surprise because this was only introduced to increase time accuracy in time-dependent problems. The FCT3 Algorithm effectively gets rid of oscillations around the discontinuity, but still creates a good deal of diffusion. The most effective results, as would be expected were produced by the FCT3ex Algorithm, mapping a sharp and monotone discontinuity. Further evidence of FCT3ex's effectiveness is given in Figure 46, where a cross-

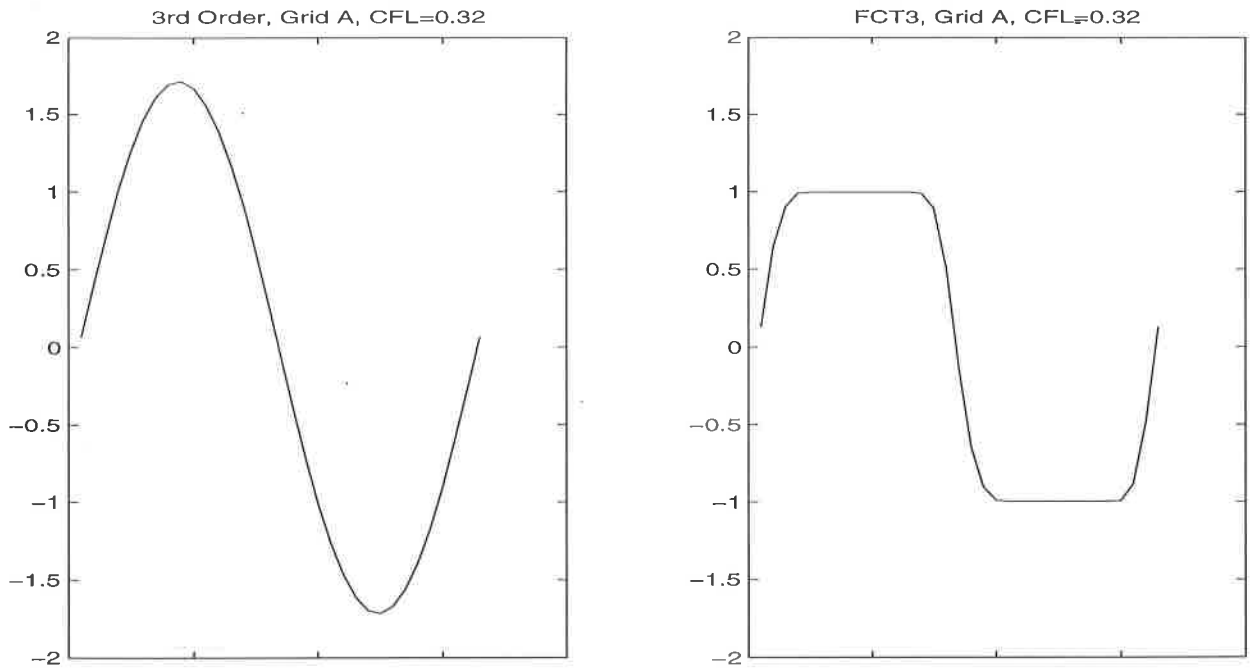

Figure 43: Cross-section of the solutions at y=0.25 at t=1.0

section through the discontinuity is shown at $y = 0.75$. This performance is what would be expected for a steady state problem.

6.5 Discussion and Further Work

The basic 3rd Order Scheme appears to have three main problems: its greater computational cost due to its extended stencil, its instabilities and its first order accuracy in time. In this chapter an attempt has been made to solve the latter two.

Applying the FCT Algorithm had problems where the entire solution was increasing/ decreasing (e.g double sine-wave case), but was very effective for the case of dampening oscillations around the discontinuity - the use for which it was originally intended. Indeed, in a time-dependent problem such as the sine-wave case, the LW Scheme has vastly superior order of accuracy (approximately 2 vs 1.25), so for such problems it would make no sense to use FCT3 instead of FCT. However, for steady state problems it is now the 3rd Order Scheme which has greater accuracy, implying that FCT3 may be more effective. But not necessarily so: if the instabilities of the scheme imply it can only be used infrequenly, the order of the overall algorithm would approach that of the PSI Scheme. For such steady problems, FCT3ex should achieve the highest order because it aims to improve on that of FCT.

Some further work would be to discover how much of an improvement this really is, and

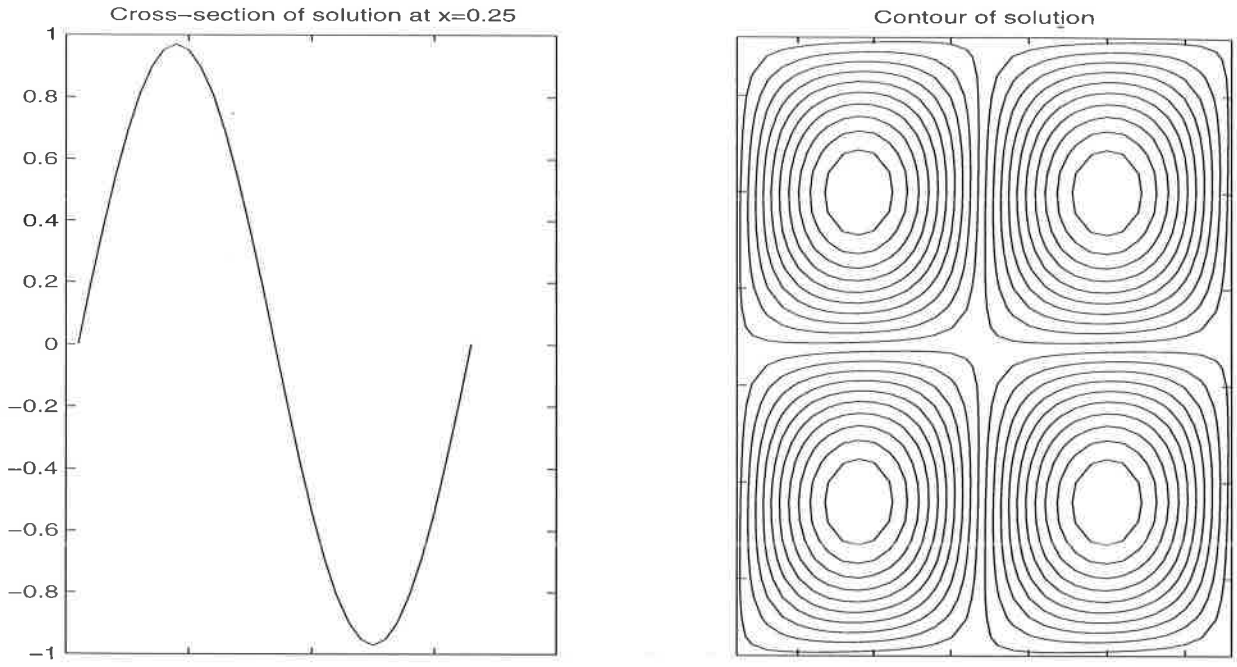

Figure 44: The Third Order Scheme using RK3 on the advecting sine curve at t=1.0

whether it be worth the extra limiting and corrector step. Other further work on FCT3ex may be to investigate the grid effects. We know the PSI and 3rd Order Schemes prefer different grid types, and LW shows very little favouritism. So what would FCT3ex prefer? More than likely this would be problem dependent, i.e. how much the algorithm depends on each of the constituent schemes for that case.

RK3 time-stepping produces excellent results for the time-dependent problems investigated in this project, producing third order accurate, stable solutions. However, the time-stepping means three times as much work per step than the LW Scheme for instance. Is the extra expense worth it in terms of the actual improvements in error over LW?

There is also scope for modifying the 3rd Order Scheme itself. The scheme doesn't obey the design criterion of continuity, with the coefficients jumping as the velocity passes over cell egdes. This is because they are dependent on in/outflow edges, and not $\vec{\lambda}$ itself. The only other scheme met in this project with a similar characteristic was Jameson's central scheme, which again needed RK time-stepping for stability. One source of experimentation would be to vary the coefficients inside and/or outside the cell in an LDA/PSI type way. Indeed, initial attempts at varying the coefficients inside the cells in an area/LDA-type way has shown some promise. Also it may be worth looking at the initial derivation of the scheme in a search for stability. Possibly a Taylor Series truncated to a higher order in time could be used, second order, or even third order creating a truely third order, one step scheme, equivalent to that of

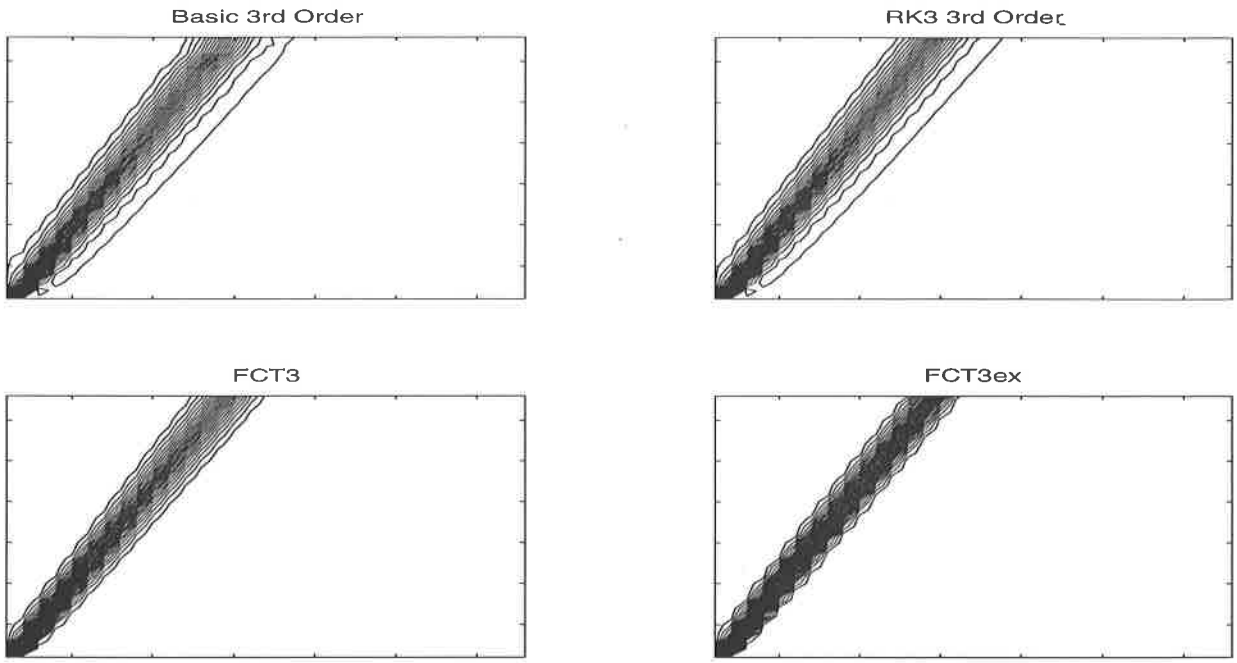

Figure 45: The discontinuous solution on Grid A

the second order LW Scheme. In fact using this technique is one way of looking at LW coming out of Jameson's scheme. However, inevitably far more nodes will be required to satisfy such accuracy leading to a far larger stencil and greater expense.

7 Conclusions

Many triangular based fluctuation distribution schemes, with an upwind bias, have been proposed over the last 15 years, with the most universally acclaimed being mentioned in Chapter 2. Their similarities with FV and FE methods have also been widely explored and have provided a basis for the evolution of more complex and accurate methods. It must be stressed that although only scalar advection is investigated in this project, the motivation behind such schemes is their applicability to systems of conservation laws derived from physical modelling e.g. Shallow Water Equations.

Solving over quadrilateral grids is an area of increasing interest, having a large influence over an admittedly small area. In the context of the project they stimulate a study into basic grid adaption and whet the appetite for nodal grid movement algorithms.

The investigations of the new 3rd Order Scheme was always going to be interesting as well as challenging, the problem in general being that the instabilities were of a far more global nature than the occasional oscillations of the linear LP schemes. FCT3, although stabilising

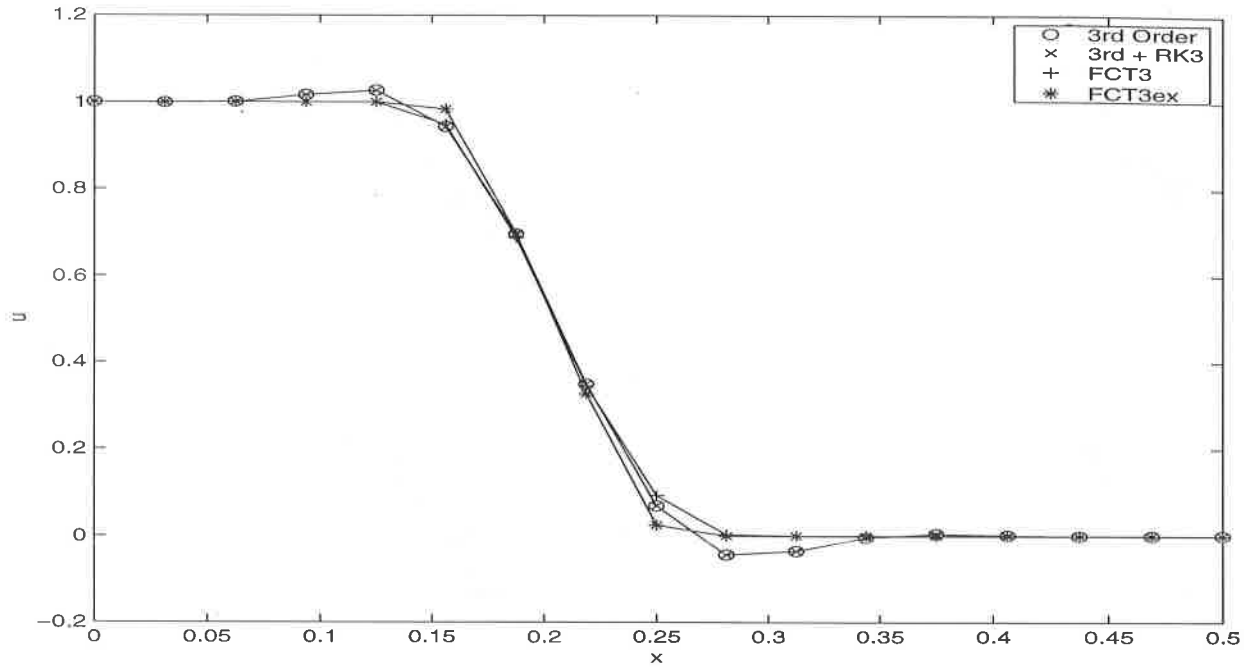

Figure 46: Cross-section through the discontinuity at y=0.75

the time-dependent problem, distorted it immeasurably. However, for the simpler, steady state problem, the results, and more so those of the FCT3ex Algorithm, were far more pleasing.

Most satisfaction however was brought about with the addition of the RK time-stepping, bringing about genuine third order accuracy for time-dependent problems.

A Equivalence of the N, NQ and DS Schemes

The object of the appendix is to show an equivalence between the N Scheme on structured triangles and the NQ and DS Schemes on the underlying square mesh, depending on the direction of the diagonals.

Suppose first, that $\vec{\lambda} = (a, b)^T$, where $0 < a < b$, $\triangle x = \triangle y = l$, and that the node u_5 is being updated.

A.1 Square grid

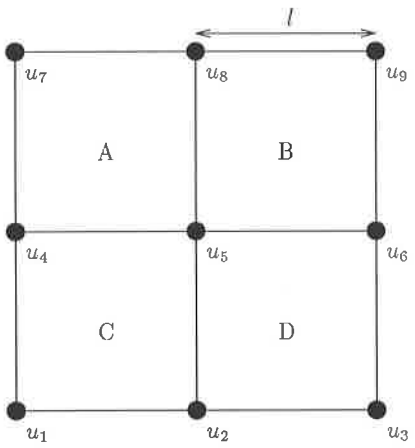

Figure 47: The stencil for the square grid.

DS Scheme :

$$\begin{aligned} u_5^{n+1} &= u_5^n + \frac{\Delta t}{S_i}\Big(\text{contributions from A,C and D}\Big) \\ &= u_5^n + \frac{\Delta t}{S_i}\left(\frac{1}{2}\vec{\lambda}.\begin{pmatrix}0\\l\end{pmatrix}(u_2-u_5) + \frac{1}{2}\vec{\lambda}.\begin{pmatrix}l\\0\end{pmatrix}(u_4-u_5) + \frac{1}{2}\vec{\lambda}.\begin{pmatrix}0\\l\end{pmatrix}(u_2-u_5) + \frac{1}{2}\vec{\lambda}.\begin{pmatrix}l\\0\end{pmatrix}(u_4-u_5)\right) \\ &= u_5^n + \frac{\Delta t}{lxl}\left(\begin{pmatrix}a\\b\end{pmatrix}.\begin{pmatrix}0\\l\end{pmatrix}(u_2-u_5) + \begin{pmatrix}a\\b\end{pmatrix}.\begin{pmatrix}l\\0\end{pmatrix}(u_4-u_5)\right) \\ &= u_5^n + \frac{\Delta t}{l}\Big(a(u_4-u_5) + b(u_2-u_5)\Big) \end{aligned} \tag{26}$$

NQ Scheme :

$$\begin{aligned} u_5^{n+1} &= u_5^n + \frac{\Delta t}{S_i}\Big(\text{contributions from C and D}\Big) \\ &= u_5^n + \frac{\Delta t}{lxl}\left(\left(\frac{1}{2}\vec{\lambda}.\begin{pmatrix}0\\l\end{pmatrix} + \frac{1}{2}\vec{\lambda}.\begin{pmatrix}-l\\0\end{pmatrix}\right)(u_2-u_5) + \left(\frac{1}{2}\vec{\lambda}.\begin{pmatrix}l\\0\end{pmatrix}\frac{1}{2}\vec{\lambda}.\begin{pmatrix}-l\\0\end{pmatrix}\right)(u_1-u_5)\right. \end{aligned}$$

$$
\begin{aligned}
&+\left(\frac{1}{2}\vec{\lambda}.\begin{pmatrix}0\\ l\end{pmatrix}\frac{1}{2}\vec{\lambda}.\begin{pmatrix}-l\\ 0\end{pmatrix}\right)(u_2-u_5)\Bigg)\\
&= u_5^n+\frac{\Delta t}{l}\Bigg((b-a)(u_2-u_5)+a(u_1-u_5)\Bigg)\\
&= u_5^n+\frac{\Delta t}{l}\Bigg(a(u_1-u_2)+b(u_2-u_5)\Bigg)
\end{aligned}
\tag{27}
$$

A.2 Triangular grid

Taking the triangulation Grid Type A, whereby the diagonals are in the same direction as the flow,

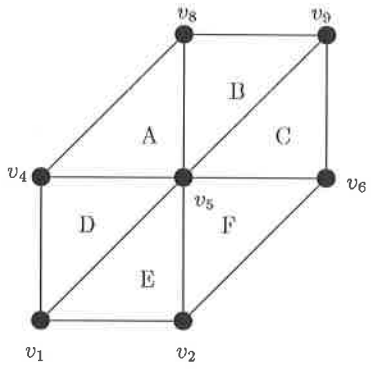

Figure 48: Grid Type A.

N Scheme :

$$
\begin{aligned}
u_5^{n+1} &= u_5^n+\frac{\Delta t}{S_i}\Bigg(\text{contributions from D, E and F}\Bigg)\\
&= u_5^n+\frac{\Delta t}{l\text{x}l}\Bigg(-\frac{1}{2}al(u_5-u_1)+\frac{1}{2}alu_1-\frac{1}{2}l(a-b)u_2-\frac{1}{2}blu_5-\frac{1}{2}l(b-a)(u_5-u_2)\Bigg)\\
&= u_5^n+\frac{\Delta t}{l}\Bigg(a(u_1-u_2)+b(u_2-u_5)\Bigg)
\end{aligned}
\tag{28}
$$

Next, taking the triangulation Grid Type C, whereby the diagonals are in the opposite direction to the flow,

N Scheme :

$$
u_5^{n+1} = u_5^n+\frac{\Delta t}{S_i}\Bigg(\text{contributions from D, E and A}\Bigg)
$$

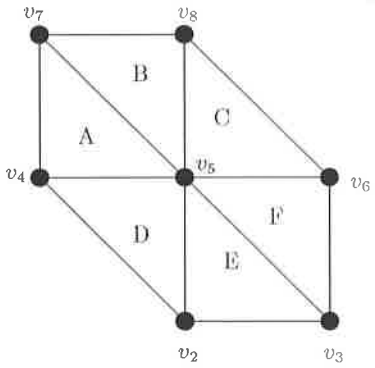

Figure 49: Grid Type C.

$$\begin{aligned} &= u_5^n + \frac{\Delta t}{l\text{x}l}\left(\frac{1}{2}blu_2 - \frac{1}{2}(a+b)lu_5 + \frac{1}{2}alu_4 - \frac{1}{2}bl(u_5-u_2) - \frac{1}{2}al(u_5-u_4)\right) \\ &= u_5^n + \frac{\Delta t}{l}\left(a(u_4-u_5) + b(u_2-u_5)\right) \end{aligned} \tag{29}$$

So, (27) and (28), as well as (26) and (29) are equivalent. Hence it has been shown that on structured triangles, when the diagonals are in the same direction as the flow then N Scheme is equivalent to the NQ Scheme on the underlying quare grid. Whilst using the N Scheme with the diagonals facing the opposite way to the flow gives the DS Scheme on the squares.

B Derivation of the Limiters γ^j

The object of this appendix is to show how to obtain the limiters γ^j for the FCT3ex Algorithm introduced in 6.3.1. The work follows the ideas of [7] and [9].

1. Let $u_i^{\max\atop\min}$ be the local max/min of u as used in the original FCT Algorithm (see one of the avove two papers for details).

2. Define
$$S_i^{\pm} = \sum_{j\in\triangle_i,\,\beta^j=1} \max\atop\min(0,\text{CEC}_i^j)$$
$$R_i^{\pm} = u_i^{\max\atop\min} - u_i^{FCT}$$

3. Let
$$T_i^{\pm} = \begin{cases} \min(1, \frac{R_i^{\pm}}{S_i^{\pm}}) & \text{if } S_i^+ > 0\,,\ S_i^- < 0 \\ 0 & \text{if } S_i = 0 \end{cases}$$

4. If $\beta^j = 1$, then,

(a)

$$\gamma_i^j = \begin{cases} T_i^+ & \text{if } \mathrm{CEC}_i^j \geq 0 \\ T_i^- & \text{if } \mathrm{CEC}_i^j < 0 \end{cases}$$

(b) $$\gamma^j = \min_{i-1,2,3}(\gamma_i^j)$$

References

[1] P.L.Roe. Fluctuations and signals - A framework for the numerical evolution problems. In K.W.Morton and M.J.Baines (editors), *Numerical Methods for Fluid Dynamics*, Institute of Mathematics and its Applications Conference Series, 219-257. Academic Press, 1982.

[2] P.L.Roe and D.Sidilkover. Optimum positive linear schemes for advection in 2 or 3 dimensions, *SIAM Journal on Numerical Analysis*, 29:(6)1542-1568, December 1992.

[3] S.K.Godunov. A finite-difference method for the computation of discontinuous solutions of the equations of fluid dynamics, *Mat. Sbornik*, 47:357-393, 1959.

[4] P.K.Sweby. High resolution schemes using flux limiters for the hyperbolic conservation laws, *SIAM Journal on Numerical Analysis*, 21:(5)995-1011, October 1984.

[5] J.März. Improving time accuracy for residual distribution schemes, *von Karman Institute for Fluid Dynamics*, Project Report 1996-17, June 1996.

[6] J.P.Boris and D.L.Book. Flux corrected transport, I, SHASTA, A fluid transport algorithm that works, *J. Comp. Phys.*, 11:38-69, 1973.

[7] J.P.Boris and D.L.Book. Flux-corrected transport III, minimal-error FCT algoritms, *J. Comp. Phys.*, 20:397-431, 1975.

[8] S.T.Zalesak. Fully multidimensional flux-corrected transport algorithms for fluids, *J. Comp. Phys.*, 31:335-363, 1978.

[9] M.E.Hubbard and P.L.Roe. Compact high-resolution algorithms for time-dependent advection on unstructured grids, *International Journal for Numerical Methods in Fluids*, 33:(5)711-736, July 2000.

[10] P.L.Roe, H.Deconinck and R.J.Struijs. Recent progress in multidimensional upwinding, *von Karman Institute for Fluid Dynamics*, Preprint 1990-32/AR, presented at 12th Int. Conf. on Numerical Methods in Fluid Dynamics, Oxford 1990.

[11] H.Deconinck, R.Struijs, G.Bourgois and P.L.Roe. Compact advection schemes on unstructured grids, *VKI Lecture Series on Comp. Fluid Dynamics*, VKI LS 1993-04, 1993.

[12] P.L.Roe. Multidimensional upwinding: motivation and concepts, *VKI Lecture Series on Comp. Fluid Dynamics*, VKI LS 1994-04, 1994.

[13] J.C.Carette, H.Deconinck and H. Paillere. Multidimensional upwinding: Its relation to finite elements, *International Journal for Numerical Methods in Fluids*, 20:935-955, 1995.

[14] R.Sruijs, P.L.Roe and H.Deconinck. Fluctuation splitting schemes for the 2D Euler equations, *VKI Lecture Series on Comp. Fluid Dynamics*, VKI LS 1991-01, 1991.

[15] H.Paillere, H.Deconinck and A.Bonfiglioli. A linearity-preserving wave-model of the solution of the Euler equations on unstructured meshes, *Proc. 2nd Eur. CFD Conf.*, Stuttgart, 1994.

[16] H.Deconinck, R.Struijs, G.Bourgois and P.L.Roe. High resolution shock capturing cell vertex advection schemes for unstructured grids, *VKI Lecture Series on Comp. Fluid Dynamics*, VKI LS 1994-05, 1994.

[17] A.Jameson and D.Mavriplis. Finite volume solution of the two-dimensional Euler equations on a regular triangular mesh, *AIAA Journal*, 24(4):611-618, 1986.

[18] A.Brooks and T.J.R.Hughes. Streamline upwind/Petrov-Galerkin formulations for the convection-dominated flows with particular emphasis on the incompressible Navier-Stokes equations, *Comp. Meths. in Appl. Mech. and Eng.*, 32:199-259, 1982.

[19] C.Johnson. Finite elements for flow problems, in *Unstructured Grid Methods for Advection Dominated Flows*, volume AGARD-R-787, 1992.

[20] A.Harten. IIigh resolution schemes for hyperbolic conservation laws, *J. Comp. Phys.*, 49:357-393, 1983.

[21] C.W.Shu and S.Osher. Efficient implementation of essentially non-oscillatory shock-capturing schemes, II, *J. Comp. Phys.*, 142(2):304-330, 1988.

[22] E.van der Weide and H.Deconinck. Fluctuation splitting schemes on quadrilateral grids. In *Proc. of the 5th ICFD Conf. on Numerical Methods in Fluids*, 1995.

[23] P.L.Roe. Optimum upwind advection on a triangular mesh, *ICASE Report*, 90-75, October 1990.

[24] K.G.Powell and B.van Leer. *AIAA-89-0095*, 1989.

[25] M.A.Rudgyard. A comparison of multidimensional upwinding for cell vertex schemes on triangular meshes. In *Numerical Methods for Fluid Dynamics V*, 1992.

[26] S.J.Leary. Least-squares methods with adjustable nodes for steady hyperbolc PDEs, *University of Reading*, PhD thesis, December 1999.

[27] P.L.Roe. Compound of many simples: Reflections on the role of model problems in CFD, in *Barriers and Challenges in Computational Fluid Dynamics*, V.Venkatakrishnan, M.D.Salas and S.R.Chakravarthy (editors), 241-258, Kluwer Academic Publishers, 1998.

[28] M.J.Baines, S.J.Leary and M.E.Hubbard. A finite volume method for steady hyperbolic equations, in *Finite Volumes for Complex Applications II*, E.Vilsmeier, F.Benkhaldoun and D.Hanel (editors), 787-794, Hermes, 1999.

[29] M.E.Hubbard. Multidimensional upwinding and grid adaption for conservation laws, *University of Reading*, PhD thesis, February 1996.